CERN-EP-2024-245
16 Sep 2024

Exposing the parton-hadron transition within jets with energy-energy correlators in pp collisions at $\sqrt{s} = 5.02$ TeV

ALICE Collaboration*

Abstract

This paper presents a fully-corrected measurement of the energy-energy correlator (EEC) within jets in pp collisions. The EEC traces the energy flow as a highly energetic parton undergoes a QCD shower followed by the confinement of partons into hadrons, probing the correlation function of the energy flow inside jets. The EEC observable is measured as a function of the charged particle pair angular distance, R_L , for $20 < p_T^{\text{ch jet}} < 80$ GeV/c. In the perturbative region (large R_L), a good agreement between the data and a next-to-leading-log perturbative QCD calculation is observed. In the non-perturbative region (small R_L), the data exhibits a linear R_L dependence. There is a transition region in between, characterized by a turnover in the EEC distribution, corresponding to the confinement process. The peak of this transition region is located at 2.42 ± 0.17 GeV/c/ $\langle p_T^{\text{ch jet}} \rangle$ for jets of various energies, indicating a common energy scale for the hadronization process. State-of-the-art Monte Carlo event generators are compared with the measurements, and can be used to constrain the parton shower and hadronization mechanisms.

arXiv:2409.12687v1 [hep-ex] 19 Sep 2024

1 Introduction

Jets serve as powerful probes for studying quantum chromodynamics (QCD). At the Large Hadron Collider (LHC), they are produced abundantly via hard scattering processes (large momentum transfer) between quarks and gluons (partons) from each colliding proton. The high-energy partons from the initial scattering undergo QCD radiation and split into lower energy partons. This process can be described using perturbative QCD (pQCD) calculations and modeled by Monte Carlo (MC) parton shower routines. Below a certain energy scale, color-neutral particles emerge when partons are confined into hadrons; eventually the final stable particles stream into detectors. The internal structure of the particles inside jets, referred to as jet substructure, encodes both the radiation pattern of the parton shower and information about the hadronization process [1]. To unravel the QCD dynamics within the fragmentation and hadronization processes, a variety of jet substructure observables have been studied [2–36]. Measurements of the jet substructure offer new opportunities for studying the properties of nuclei and the quark–gluon plasma (QGP) via the interplay between the jet and the cold or the hot QCD medium in proton–nucleus (pA) and nucleus–nucleus (AA) collisions, respectively [37–39].

A novel jet substructure observable, referred to as energy-energy correlator (EEC) [40–42], focuses on the correlation function of energy flow inside jets. Originally introduced as an event shape observable in e^+e^- collisions [43–46] or as the observable needed to construct jet discriminators [47–49], the EEC is infrared-collinear (IRC) safe [50] and can be calculated from first principles in QCD in the perturbative limit [46]. It has been used to constrain the strong coupling constant α_s [44–46]. EEC observables can be defined in different ways, offering precision probes of both perturbative and non-perturbative QCD dynamics in collisions ranging from e^+e^- annihilation and hadronic collisions, to deep inelastic scattering (DIS), as summarized in Ref. [51].

Experimentally, the EEC is an energy-weighted two-particle correlation as a function of the angular distance between pairs of particles. In this paper, we study the EEC inside high-energy jets produced in pp collisions at $\sqrt{s} = 5.02$ TeV. This approach focuses on the energy correlation function in the collinear limit instead of over the whole event, providing a new perspective on jet evolution, from perturbative splittings to parton confinement into hadrons [40]. The energy-energy correlation function, $\Sigma_{\text{EEC}}(R_L)$, is defined as the following:

$$\Sigma_{\text{EEC}}(R_L) = \frac{1}{N_{\text{jet}} \cdot \Delta} \int_{R_L - \frac{1}{2}\Delta}^{R_L + \frac{1}{2}\Delta} \sum_{\text{jets}} \sum_{i,j} \frac{p_{T,i} p_{T,j}}{(p_T^{\text{jet}})^2} \delta(R'_L - R_{L,ij}) dR'_L. \quad (1)$$

The sum runs over all final state particle pairs (i, j) inside each jet ¹. The angular distance between each pair in the $\eta - \phi$ plane is $R_{L,ij} = \sqrt{(\phi_j - \phi_i)^2 + (\eta_j - \eta_i)^2}$. Δ is the angular bin width and N_{jet} is the total number of jets. Figure 1 illustrates how particles inside a jet are paired when constructing the EEC observable.

Recent theoretical developments have enabled the analytical calculation of energy correlators inside jets to high accuracy [40], and the calculation has been extended to charged particles using track functions [42, 52–55]. As the soft radiation is suppressed by the energy weight, this observable has reduced sensitivity to higher-order corrections, the underlying event, and soft jet fragments in the perturbative regime.

Another unique advantage of the EEC observable arises from the angular scale, R_L . Based on the angular ordering of the QCD radiation (splitting), the time scale τ of splitting can be approximated by $\tau \sim 1/(p_T^{\text{jet}} \cdot R_L^2)$, where τ is the splitting time and p_T^{jet} represents the scale of the initial hard process [40, 41]. The large- R_L regime corresponds to the perturbative regime during the early parton splitting stage of the jet dynamics, hence referred to as the perturbative or parton scaling region. Non-perturbative effects become more significant as the QCD radiation evolves towards lower energy scales and smaller angles. At a certain angular scale, confinement is expected to take place. This separation of the perturbative

¹Both pair (i, j) and (j, i) are considered. For example, a pair of particle 1 and particle 2 is counted twice, $(1, 2)$ and $(2, 1)$.

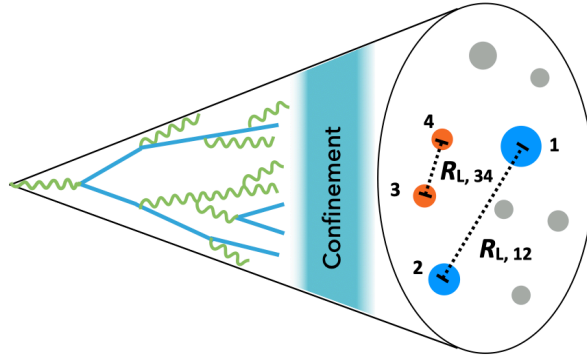


Figure 1: A schematic of the jet evolution through parton shower (lines), confinement process (shaded area), to final state particles (circles).

and non-perturbative regimes into distinct angular regions was already observed by the CMS experiment [41, 56], and they have extracted α_s to high precision using the energy correlators in the perturbative regime.

In the paper we take advantage of the excellent track reconstruction capabilities of the ALICE experiment [38] to construct the EEC using charged particle tracks within reconstructed charged-particle jets. The measurement of jet EEC in pp collisions with detector effects fully corrected at the LHC is presented. The measurements are reported in charged particle jet p_T ($p_T^{\text{ch jet}}$) intervals of 20–40, 40–60, 60–80 GeV/ c , which marks the first EEC measurement in jets in such a low- p_T kinematic regime. The results are compared with state-of-the-art MC models with different hadronization mechanisms and pQCD calculations. The transition region is analyzed to study hadronization as a function of jet p_T .

2 Experimental setup and data sets

This analysis utilizes pp collisions at $\sqrt{s} = 5.02$ TeV collected by the ALICE experiment in 2017. Minimum bias events are triggered by coincidence hits on the V0 scintillator detectors [57] at forward and backward rapidity. Events are required to have a primary vertex within ± 10 cm of the nominal interaction point to provide uniform acceptance and high tracking efficiency. Events with more than one reconstructed collision vertex are removed to avoid pileup of multiple collisions. A total of 870 million minimum bias events passed the event selection criteria, corresponding to an integrated luminosity of $18.0 \pm 0.4 \text{ nb}^{-1}$ [58].

The central barrel tracking system is the main detector used in this analysis. The central tracker consists of the Inner Tracking System (ITS) [59] and Time Projection Chamber (TPC) [60]. They are inside a 0.5 T magnetic field and have a high efficiency for detection of charged particles with p_T ($p_{T,\text{track}}$) from 0.15 to 100 GeV/ c , $|\eta| < 0.9$, and $0 < \varphi < 2\pi$. The single track efficiency is p_T dependent, increasing from $\sim 60\%$ at 0.15 GeV to $\sim 80\%$ at 1 GeV and remaining above 75% at higher p_T . The momentum resolution, σ_p/p , is $\approx 1\%$ at $p_{T,\text{track}} = 1$ GeV/ c increasing to $\approx 4\%$ at $p_{T,\text{track}} = 4$ GeV/ c . The angular resolution is ≈ 1 mrad at $p_{T,\text{track}} = 1$ GeV/ c decreasing to < 0.6 mrad for $p_{T,\text{track}} > 5$ GeV/ c . More detailed descriptions of the ALICE detector and performance can be found in Ref. [61, 62].

3 Analysis method

Charged particles measured by the central barrel tracking system are selected using the same criteria as in Ref [61, 63]. The selected charged particles are clustered into jets via the anti- k_T algorithm with $R = 0.4$ using the FastJet 3.3.3 package [64]. The E-scheme recombination is used, assigning all charged particles the pion mass. Reconstructed jets with $|\eta_{\text{jet}}| < 0.9 - R$ are used to avoid detector edge effects in the jet reconstruction. The EEC observable is measured in charged jet p_T ranges of $20 < p_T^{\text{ch jet}} < 40$ GeV/ c , $40 < p_T^{\text{ch jet}} < 60$ GeV/ c , and $60 < p_T^{\text{ch jet}} < 80$ GeV/ c . Only constituents inside the reconstructed jets with

$p_{T,\text{track}} > 1$ GeV/ c enter the EEC, in order to reduce the impact of non-jet particles from the underlying event (UE). No additional corrections are applied for the presence of the UE.

Detector effects are assessed by simulating pp collisions with PYTHIA 8 (version 8.210) [65] Monash tune [66] and then propagating the final-state particles through a GEANT3 model [67] of the ALICE detector. The key detector effects for EEC are the track momentum resolution, angular resolution, and efficiency for both single tracks and track pairs. The track momentum resolution and efficiency affect the calculated energy weights, the number of reconstructed pairs, and the reconstructed $p_T^{\text{ch,jet}}$. Track pairs at very small angular separation with the same charge have very similar trajectories in the tracking volume, which may cause the track reconstruction algorithm to miss one of the tracks or mis-reconstruct them. This effect is referred to as the track-merging effect, and was quantified for the femtoscopy measurements in ALICE [68]. Track merging decreases the pair efficiency for tracks at small distance, causing a reduced Σ_{EEC} at low R_L . A $\sim 90\%$ pair efficiency is observed in the GEANT simulation for pairs with $R_L > 0.01$, which drops steeply to $< 20\%$ for pairs with smaller R_L . To achieve precise measurements with small systematic uncertainties, results are reported for $R_L > 0.01$.

The values of the corrections are $< 10\%$, except for the R_L bins near 0.01, for which the corrections are about 20%. As each track pair has a unique energy weight, full unfolding to correct for detector effects is complicated and requires higher statistics. However, the excellent momentum and position resolution in ALICE results in little bin migration in R_L . Hence, in this analysis, instead of unfolding, a two-dimensional bin-by-bin correction is utilized where the correction factors are obtained from the simulation by comparing the generator-level and corresponding detector-level information for each $p_T^{\text{ch,jet}}$ and R_L bin. The bin-by-bin correction can be more sensitive to differences between the generator used for deriving the correction factor and the physics events collected; this is included in the systematic uncertainty. A cross-check was performed using a Bayesian unfolding technique [69, 70]. The difference between the unfolded and bin-by-bin corrected EEC distributions is small and is included in the systematic uncertainties.

4 Systematic uncertainties

The main systematic uncertainty sources in this measurement are the single-track efficiency, the track pair efficiency, the generator dependence of the correction factors and the unfolding cross check. The single-track efficiency uncertainty is estimated to be $\approx 3\%$ based on previous studies where the track selection and ITS-TPC matching criteria are varied [71]. The impact of this uncertainty is determined by randomly rejecting 3% of the detector-level tracks in simulated events and re-calculating the correction factors. It leads to a R_L dependent change of $\leq 3\%$, which is quoted as the systematic uncertainty for single-track efficiency and also includes the track efficiency uncertainty effect upon the jet p_T . The systematic uncertainty due to the pair efficiency is evaluated by studying the variation of the corrected data points with different pair selection parameters, yielding $\leq 2\%$ variation in the R_L range reported. The uncertainty from the generator dependence of the correction factors is determined by comparing the correction factors extracted from events simulated with PYTHIA 8 [71] and Herwig 7 [72], with parameterized detector responses included, yielding $\leq 2\%$ variation. The unfolded EEC shows $\leq 4\%$ difference from the bin-by-bin corrected results, and the difference is assigned as a systematic uncertainty on the bin-by-bin correction method. The systematic uncertainties are assumed to be independent and are added in quadrature, resulting in a total uncertainty of $< 6\%$.

5 Results and discussion

The EEC distributions for $p_T^{\text{ch,jet}}$ ranges of 20–40, 40–60, and 60–80 GeV/ c are shown in the top panels of Fig. 2. In each $p_T^{\text{ch,jet}}$ range, distinct R_L dependences are observed at the large-angle and small-angle limits, with a transition region in between. The three regions can be intuitively understood with the following explanations:

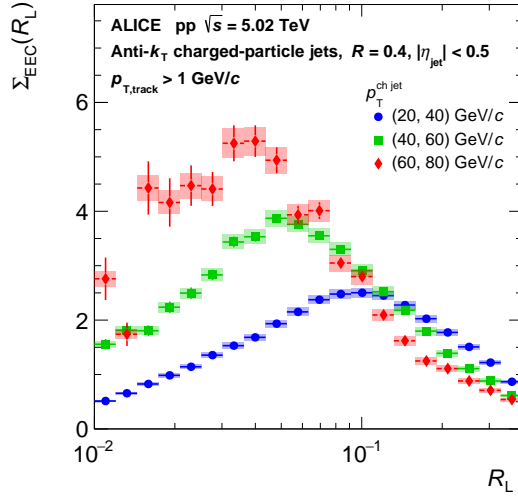


Figure 2: Fully corrected Σ_{EEC} as a function of R_L in the $p_T^{\text{ch jet}}$ intervals 20–40, 40–60, and 60–80 GeV/c.

- The region at large R_L (partonic degrees of freedom) is determined by the early time jet evolution where partons split and shower perturbatively. Harder splittings with a larger R_L occur less often than soft emissions with a smaller R_L .
- The region at small R_L (hadronic degrees of freedom) reflects the jet structure at later times dominated by the features of QCD inaccessible with perturbative methods. Hadron pairs with a smaller R_L occur less often as the phase space reduces.
- The intermediate R_L transition region, marked by a peak structure between the non-perturbative and pQCD regions, is a signature of the hadronization process, where partons are confined into colorless hadrons.

The EEC distributions exhibit a significant jet p_T dependence, even within the limited range of jet momenta in this work. For jets in the higher $p_T^{\text{ch jet}}$ range, the perturbative region extends to smaller R_L values, consequently shifting the peak of the transition region to a lower R_L . This behavior is expected since the energy scale or virtuality, μ , of the parton splitting is proportional to the product of the jet p_T and R_L . Hadronization occurs when μ approaches the hadronization energy scale Λ . At this point, parton splitting ceases and the Σ_{EEC} stops increasing. As a result, the transition peak should be located at $R_L \sim \Lambda/p_T^{\text{ch jet}}$ [73, 74], implying that the EEC in more energetic jets peaks at smaller angular scales, consistent with our observations.

To further examine the dependence of the transition region on the energy of jets, the peak position (R_L^{peak}) and peak height ($\Sigma_{EEC}^{\text{peak}}$) are extracted for the measured $p_T^{\text{ch jet}}$ ranges (see Appendix A). We find that R_L^{peak} is proportional to $1/\langle p_T^{\text{ch jet}} \rangle$ and $\Sigma_{EEC}^{\text{peak}}$ is proportional to $\langle p_T^{\text{ch jet}} \rangle / \ln \langle p_T^{\text{ch jet}} \rangle^2$. $\langle p_T^{\text{ch jet}} \rangle$ is the average p_T for charged-particle jets in each p_T bin, extracted from PYTHIA 8 (Monash tune) reweighted to reproduce the ALICE data in Ref. [71]. To directly visualize the jet p_T dependence of the transition peak position and height, Σ_{EEC} as a function of $\langle p_T^{\text{ch jet}} \rangle R_L$ is shown in Fig. 3. The vertical scale of the EEC distribution is scaled by $\ln \langle p_T^{\text{ch jet}} \rangle / \langle p_T^{\text{ch jet}} \rangle$. Strikingly, the scaled EEC distributions, $\ln \langle p_T^{\text{ch jet}} \rangle / \langle p_T^{\text{ch jet}} \rangle \Sigma_{EEC}$, for different $p_T^{\text{ch jet}}$ bins collapse into a common curve.

At large R_L , a next-to-leading-logarithmic (NLL) pQCD calculation [42] is shown in the orange curve. The overall magnitude of the pQCD curve is normalized to data in the large-angle region where $\langle p_T^{\text{ch jet}} \rangle R_L \gg$

² The $\langle p_T^{\text{ch jet}} \rangle$ inside $\ln \langle p_T^{\text{ch jet}} \rangle$ actually represents $\langle p_T^{\text{ch jet}} \rangle / (\text{GeV}/c)$, which is a unit-less number. For simplicity in notation, we use $\ln \langle p_T^{\text{ch jet}} \rangle$ for $\ln(\langle p_T^{\text{ch jet}} \rangle / (\text{GeV}/c))$ throughout this paper.

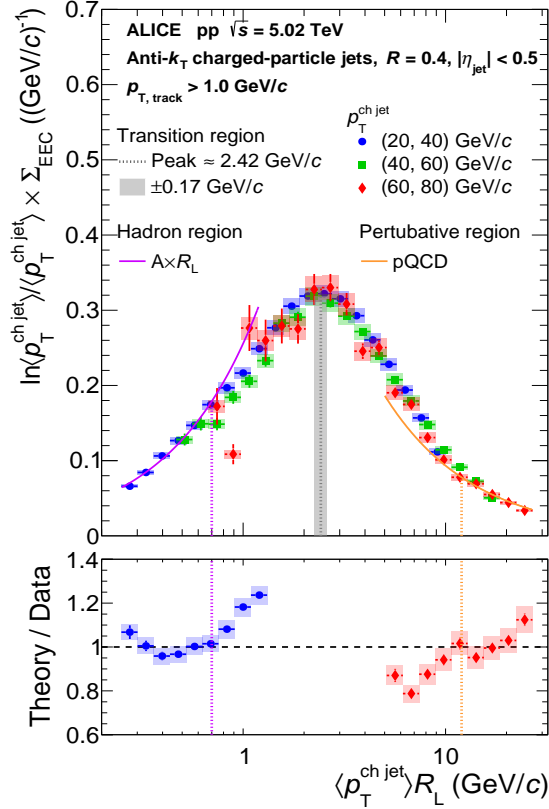


Figure 3: Normalized Σ_{EEC} as a function of $\langle p_T^{\text{ch jet}} \rangle R_L$. $\ln(\langle p_T^{\text{ch jet}} \rangle)$ in the y-axis represents $\ln(\langle p_T^{\text{ch jet}} \rangle / (\text{GeV}/c))$ as explained in footnote 2. The gray line corresponds to the maximum location of the distribution and the gray band corresponds to a ± 0.17 GeV/c uncertainty along the x-axis. The orange curves show pQCD calculations [42], which are normalized to data such that the integral inside R_L range of $[12 \text{ GeV}/c / \langle p_T^{\text{ch jet}} \rangle, 0.4]$ are the same. The purple curve represents a linear functional form that is fit to data in the R_L range of $[0.01, 0.7 \text{ GeV}/c / \langle p_T^{\text{ch jet}} \rangle]$. Bottom: Ratios of the pQCD calculation and linear fit to data. As the fitting range for the linear curve is mostly accessible by the data in 20–40 GeV/c, the ratio of linear fit to data is only shown for 20–40 GeV/c. As the normalization range for the orange pQCD curve is mostly accessible by the data in 60–80 GeV/c, the ratio of pQCD to data is only shown for 60–80 GeV/c.

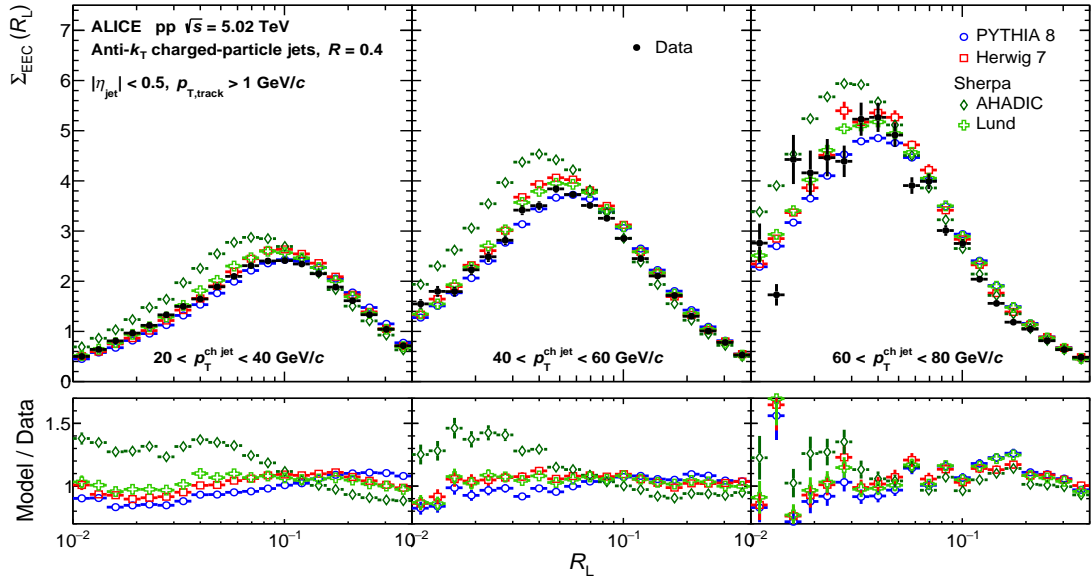


Figure 4: Top: Fully corrected Σ_{EEC} as a function of R_L . Bottom: Ratio of Σ_{EEC} from MC event generators to data.

Λ_{QCD} [42]. The normalization range is R_L between $12 \text{ GeV}/c/\langle p_T^{\text{ch jet}} \rangle$ and 0.4 (jet radius), which is accessible in the measured EEC distribution of the 60–80 GeV/c range. Inside this R_L range, a good shape agreement is observed between the pQCD prediction and the measurement, except for the last point where R_L approaches the jet radius. At smaller R_L , the data deviate from perturbative scaling, which is expected as non-perturbative effects like soft radiation and hadronization become important. Recent theoretical studies show that power corrections for non-perturbative effects [75, 76] can be added to pQCD calculations, which extend the description of EEC measurements to smaller angles.

After the transition region where a broad peak structure is observed, the data follow a different R_L dependence at very small R_L . This is well described by a linear function in R_L , shown by the purple curve in Fig. 3. The linear function is fit to the EEC distribution of 20–40 GeV/c in R_L range of $[0.01, 0.7 \text{ GeV}/c/\langle p_T^{\text{ch jet}} \rangle]$. Linear scaling is expected if the energy is uniformly distributed, where the correlation strength depends only on the area of the infinitesimal ring at distance R_L and is thus proportional to $R_L dR_L$. The correlation of such EEC pairs are purely combinatorial as would be the case for freely moving (non-interacting) hadrons. Therefore, the small- R_L region is often referred to as non-perturbative or free hadron scaling region [41, 56, 56]. This linear dependence breaks down towards larger angles as impacted by the correlations induced by hadronic interactions (including formation and decay from excited states), hadronization, and eventually parton splittings dominating the high- R_L region.

The maxima of the transition peaks coincide at $\langle p_T^{\text{ch jet}} \rangle R_L = 2.42 \pm 0.17 \text{ GeV}/c$. This observation implies a common energy scale for the hadronization process where QCD radiations stop, independent of the jet energy. Interestingly, the transition peak position is not affected by lowering the $p_{T,\text{track}}$ selection to 0.15 GeV/c for the measured $p_T^{\text{ch jet}}$ range (see Appendix B). The shape of the transition region in Fig. 3 is also independent of jet energy, up to 80 GeV/c - the highest p_T accessible with our data sample.

Figure 4 compares the measured EEC distributions and the MC models PYTHIA 8 (Monash tune) [77], Herwig 7 (default tune) [72], and Sherpa 2.2.15 [78]. The default parton shower models are used for PYTHIA 8 (p_T -ordered), Herwig 7 (angular-ordered), and Sherpa (p_T -ordered). The MC models used here implement different hadronization mechanisms. PYTHIA 8 uses the Lund string hadronization model, which produces hadrons by breaking a color string into color-neutral hadrons. Herwig 7 uses a cluster hadronization model, where locally color-connected partons are collected into clusters which then decay into hadrons. In Sherpa, the AHADIC tune uses a cluster hadronization model, while the

Lund tune uses the Lund string hadronization. Both PYTHIA 8 and Herwig 7 describe the data within 20% across the measured R_L range. The transition region peaks at a slightly larger angle in PYTHIA 8 compared to Herwig 7. Herwig 7 better describes the transition peak position, but exhibits a slightly wider transition region than the data. For Sherpa, the Lund tune agrees with the data quite well, while the AHADIC tune shows up to a 50% deviation in the small-angle region. The agreement with data improves for MC models as the jet p_T increases. When comparing the EEC distributions from Sherpa with different hadronization models to data, it is worth noting that the transition region from AHADIC (cluster hadronization) is at a smaller angle compared to the Lund tune (string hadronization). This indicates that the clustering hadronization model tends to cause a later hadronization compared to Lund string breaking. Such a shift of the transition region is also observed when comparing Herwig 7 and PYTHIA 8, where Herwig 7 shows a transition region at smaller angles compared to PYTHIA 8. The impact of the different hadronization parameters in PYTHIA 8 on the transition region of EEC distributions can be found in Appendix C. More detailed comparisons with MC models could constrain the parton shower, hadronization, and hadronic interactions in the models.

6 Conclusions

We report the EEC distributions for charged-particle jets produced in pp collisions measured with the ALICE detector. This marks the first energy correlator measurements that are fully corrected for detector effects at the LHC for low- p_T jets. The data are in good agreement with a pQCD calculation in the large angle region. Linear scaling with R_L is observed at small R_L , as expected for freely moving hadrons with uniformly distributed energy. A transition region between the two corresponds to the hadronization process. The transition region shows a clear jet energy dependence, peaking at a smaller angular scale for jets with higher p_T . The re-normalized EEC distributions as a function of $\langle p_T^{\text{ch jet}} \rangle R_L$ reveal that this quantity governs the shape of the EEC distribution, directly relating to the energy scale (virtuality) of jets. A common transition position occurs at $R_L \sim (2.4 \text{ GeV}/c) / \langle p_T^{\text{ch jet}} \rangle$.

MC models describe the data within 20% across the measured R_L range, except for Sherpa with AHADIC tune. The discrepancy between models and data decreases for jets with higher energy. As the hadronization process is a non-perturbative phenomenon, theory predictions based on first principles are challenging, and developments in lattice QCD and quantum computation may offer needed improvements [79]. In the future, measurements of higher-order energy correlators and comparison of EEC measurements from different collision systems can provide further insight on the confinement process [40, 41, 80]. The study presented in this letter provides a baseline for using EEC to study cold and hot nuclear medium effects on jet formation and propagation.

Acknowledgements

The ALICE Collaboration gratefully acknowledge Kyle Lee for providing theoretical predictions. The ALICE Collaboration would like to thank all its engineers and technicians for their invaluable contributions to the construction of the experiment and the CERN accelerator teams for the outstanding performance of the LHC complex. The ALICE Collaboration gratefully acknowledges the resources and support provided by all Grid centres and the Worldwide LHC Computing Grid (WLCG) collaboration. The ALICE Collaboration acknowledges the following funding agencies for their support in building and running the ALICE detector: A. I. Alikhanyan National Science Laboratory (Yerevan Physics Institute) Foundation (ANSL), State Committee of Science and World Federation of Scientists (WFS), Armenia; Austrian Academy of Sciences, Austrian Science Fund (FWF): [M 2467-N36] and Nationalstiftung für Forschung, Technologie und Entwicklung, Austria; Ministry of Communications and High Technologies, National Nuclear Research Center, Azerbaijan; Conselho Nacional de Desenvolvimento Científico e Tecnológico (CNPq), Financiadora de Estudos e Projetos (Finep), Fundação de Amparo à Pesquisa do Estado de São Paulo (FAPESP) and Universidade Federal do Rio Grande do Sul (UFRGS), Brazil; Bulgarian Ministry of Education and Science, within the National Roadmap for Research Infrastructures 2020-2027 (object CERN), Bulgaria; Ministry of Education of China (MOEC), Ministry of Science & Technology of China (MSTC) and National Natural Science Foundation of China (NSFC), China; Ministry of Science and Education and Croatian Science Foundation, Croatia; Centro de Aplicaciones Tecnológicas y Desarrollo Nuclear (CEADEN), Cubaenergía, Cuba; Ministry of Education, Youth and Sports of the Czech Republic, Czech Republic; The Danish Council for Independent Research | Natural Sciences, the VILLUM FONDEN and Danish National Research Foundation (DNRF), Denmark; Helsinki Institute of Physics (HIP), Finland; Commissariat à l’Energie Atomique (CEA) and Institut National de Physique Nucléaire et de Physique des Particules (IN2P3) and Centre National de la Recherche Scientifique (CNRS), France; Bundesministerium für Bildung und Forschung (BMBF) and GSI Helmholtzzentrum für Schwerionenforschung GmbH, Germany; General Secretariat for Research and Technology, Ministry of Education, Research and Religions, Greece; National Research, Development and Innovation Office, Hungary; Department of Atomic Energy Government of India (DAE), Department of Science and Technology, Government of India (DST), University Grants Commission, Government of India (UGC) and Council of Scientific and Industrial Research (CSIR), India; National Research and Innovation Agency - BRIN, Indonesia; Istituto Nazionale di Fisica Nucleare (INFN), Italy; Japanese Ministry of Education, Culture, Sports, Science and Technology (MEXT) and Japan Society for the Promotion of Science (JSPS) KAKENHI, Japan; Consejo Nacional de Ciencia (CONACYT) y Tecnología, through Fondo de Cooperación Internacional en Ciencia y Tecnología (FONCICYT) and Dirección General de Asuntos del Personal Académico (DGAPA), Mexico; Nederlandse Organisatie voor Wetenschappelijk Onderzoek (NWO), Netherlands; The Research Council of Norway, Norway; Pontificia Universidad Católica del Perú, Peru; Ministry of Science and Higher Education, National Science Centre and WUT ID-UB, Poland; Korea Institute of Science and Technology Information and National Research Foundation of Korea (NRF), Republic of Korea; Ministry of Education and Scientific Research, Institute of Atomic Physics, Ministry of Research and Innovation and Institute of Atomic Physics and Universitatea Nationala de Stiinta si Tehnologie Politehnica Bucuresti, Romania; Ministry of Education, Science, Research and Sport of the Slovak Republic, Slovakia; National Research Foundation of South Africa, South Africa; Swedish Research Council (VR) and Knut & Alice Wallenberg Foundation (KAW), Sweden; European Organization for Nuclear Research, Switzerland; Suranaree University of Technology (SUT), National Science and Technology Development Agency (NSTDA) and National Science, Research and Innovation Fund (NSRF via PMU-B B05F650021), Thailand; Turkish Energy, Nuclear and Mineral Research Agency (TENMAK), Turkey; National Academy of Sciences of Ukraine, Ukraine; Science and Technology Facilities Council (STFC), United Kingdom; National Science Foundation of the United States of America (NSF) and United States Department of Energy, Office of Nuclear Physics (DOE NP), United States of America. In addition, individual groups or members have received support from: Czech Science Foundation (grant no. 23-07499S), Czech Republic; FORTE project, reg.

no. CZ.02.01.01/00/22_008/0004632, Czech Republic, co-funded by the European Union, Czech Republic; European Research Council (grant no. 950692), European Union; ICSC - Centro Nazionale di Ricerca in High Performance Computing, Big Data and Quantum Computing, European Union - NextGenerationEU; Academy of Finland (Center of Excellence in Quark Matter) (grant nos. 346327, 346328), Finland.

References

- [1] G. P. Salam, “Towards Jetography”, *Eur. Phys. J. C* **67** (2010) 637–686, arXiv:0906.1833 [hep-ph].
- [2] ALICE Collaboration, B. B. Abelev *et al.*, “Charged jet cross sections and properties in proton-proton collisions at $\sqrt{s} = 7$ TeV”, *Phys. Rev. D* **91** (2015) 112012, arXiv:1411.4969 [nucl-ex].
- [3] ALICE Collaboration, S. Acharya *et al.*, “Jet fragmentation transverse momentum measurements from di-hadron correlations in $\sqrt{s} = 7$ TeV pp and $\sqrt{s_{NN}} = 5.02$ TeV p–Pb collisions”, *JHEP* **03** (2019) 169, arXiv:1811.09742 [nucl-ex].
- [4] ALICE Collaboration, S. Acharya *et al.*, “Charged jet cross section and fragmentation in proton-proton collisions at $\sqrt{s} = 7$ TeV”, *Phys. Rev. D* **99** (2019) 012016, arXiv:1809.03232 [nucl-ex].
- [5] ALICE Collaboration, S. Acharya *et al.*, “Measurement of the production of charm jets tagged with D^0 mesons in pp collisions at $\sqrt{s} = 7$ TeV”, *JHEP* **08** (2019) 133, arXiv:1905.02510 [nucl-ex].
- [6] ALICE Collaboration, S. Acharya *et al.*, “Exploration of jet substructure using iterative declustering in pp and Pb–Pb collisions at LHC energies”, *Phys. Lett. B* **802** (2020) 135227, arXiv:1905.02512 [nucl-ex].
- [7] ALICE Collaboration, S. Acharya *et al.*, “Measurements of the groomed and ungroomed jet angularities in pp collisions at $\sqrt{s} = 5.02$ TeV”, *JHEP* **05** (2022) 061, arXiv:2107.11303 [nucl-ex].
- [8] ALICE Collaboration, S. Acharya *et al.*, “Measurement of the groomed jet radius and momentum splitting fraction in pp and Pb–Pb collisions at $\sqrt{s_{NN}} = 5.02$ TeV”, *Phys. Rev. Lett.* **128** (2022) 102001, arXiv:2107.12984 [nucl-ex].
- [9] ALICE Collaboration, S. Acharya *et al.*, “First measurements of N-subjettiness in central Pb–Pb collisions at $\sqrt{s_{NN}} = 2.76$ TeV”, *JHEP* **10** (2021) 003, arXiv:2105.04936 [nucl-ex].
- [10] ALICE Collaboration, S. Acharya *et al.*, “Direct observation of the dead-cone effect in quantum chromodynamics”, *Nature* **605** (2022) 440–446, arXiv:2106.05713 [nucl-ex]. [Erratum: *Nature* 607, E22 (2022)].
- [11] ALICE Collaboration, S. Acharya *et al.*, “Measurement of the angle between jet axes in pp collisions at $\sqrt{s} = 5.02$ TeV”, *JHEP* **07** (2023) 201, arXiv:2211.08928 [nucl-ex].
- [12] ALICE Collaboration, S. Acharya *et al.*, “Measurement of inclusive and leading subjet fragmentation in pp and Pb–Pb collisions at $\sqrt{s_{NN}} = 5.02$ TeV”, *JHEP* **05** (2023) 245, arXiv:2204.10270 [nucl-ex].
- [13] ATLAS Collaboration, G. Aad *et al.*, “Jet mass and substructure of inclusive jets in $\sqrt{s} = 7$ TeV pp collisions with the ATLAS experiment”, *JHEP* **05** (2012) 128, arXiv:1203.4606 [hep-ex].

- [14] **ATLAS** Collaboration, G. Aad *et al.*, “ATLAS Measurements of the Properties of Jets for Boosted Particle Searches”, *Phys. Rev. D* **86** (2012) 072006, arXiv:1206.5369 [hep-ex].
- [15] **ATLAS** Collaboration, G. Aad *et al.*, “Measurement of jet shapes in top-quark pair events at $\sqrt{s} = 7$ TeV using the ATLAS detector”, *Eur. Phys. J. C* **73** (2013) 2676, arXiv:1307.5749 [hep-ex].
- [16] **ATLAS** Collaboration, M. Aaboud *et al.*, “Measurement of the Soft-Drop Jet Mass in pp Collisions at $\sqrt{s} = 13$ TeV with the ATLAS Detector”, *Phys. Rev. Lett.* **121** (2018) 092001, arXiv:1711.08341 [hep-ex].
- [17] **ATLAS** Collaboration, M. Aaboud *et al.*, “Measurement of jet-substructure observables in top quark, W boson and light jet production in proton-proton collisions at $\sqrt{s} = 13$ TeV with the ATLAS detector”, *JHEP* **08** (2019) 033, arXiv:1903.02942 [hep-ex].
- [18] **ATLAS** Collaboration, G. Aad *et al.*, “Properties of jet fragmentation using charged particles measured with the ATLAS detector in pp collisions at $\sqrt{s} = 13$ TeV”, *Phys. Rev. D* **100** (2019) 052011, arXiv:1906.09254 [hep-ex].
- [19] **ATLAS** Collaboration, G. Aad *et al.*, “Measurement of soft-drop jet observables in pp collisions with the ATLAS detector at $\sqrt{s} = 13$ TeV”, *Phys. Rev. D* **101** (2020) 052007, arXiv:1912.09837 [hep-ex].
- [20] **ATLAS** Collaboration, G. Aad *et al.*, “Measurement of the Lund Jet Plane Using Charged Particles in 13 TeV Proton-Proton Collisions with the ATLAS Detector”, *Phys. Rev. Lett.* **124** (2020) 222002, arXiv:2004.03540 [hep-ex].
- [21] **ATLAS** Collaboration, G. Aad *et al.*, “Measurement of substructure-dependent jet suppression in Pb+Pb collisions at 5.02 TeV with the ATLAS detector”, *Phys. Rev. C* **107** (2023) 054909, arXiv:2211.11470 [nucl-ex].
- [22] **ATLAS** Collaboration, G. Aad *et al.*, “Measurement of the jet mass in high transverse momentum $Z(\rightarrow b\bar{b})\gamma$ production at $\sqrt{s} = 13$ TeV using the ATLAS detector”, *Phys. Lett. B* **812** (Jan, 2021) 135991, arXiv:1907.07093 [hep-ex].
- [23] **CMS** Collaboration, S. Chatrchyan *et al.*, “Shape, Transverse Size, and Charged Hadron Multiplicity of Jets in pp Collisions at 7 TeV”, *JHEP* **06** (2012) 160, arXiv:1204.3170 [hep-ex].
- [24] **CMS** Collaboration, S. Chatrchyan *et al.*, “Measurement of jet fragmentation into charged particles in pp and PbPb collisions at $\sqrt{s_{NN}} = 2.76$ TeV”, *JHEP* **10** (2012) 087, arXiv:1205.5872 [nucl-ex].
- [25] **CMS** Collaboration, S. Chatrchyan *et al.*, “Measurement of Jet Fragmentation in PbPb and pp Collisions at $\sqrt{s_{NN}} = 2.76$ TeV”, *Phys. Rev. C* **90** (2014) 024908, arXiv:1406.0932 [nucl-ex].
- [26] **CMS** Collaboration, A. M. Sirunyan *et al.*, “Measurements of jet charge with dijet events in pp collisions at $\sqrt{s} = 8$ TeV”, *JHEP* **10** (2017) 131, arXiv:1706.05868 [hep-ex].
- [27] **CMS** Collaboration, A. M. Sirunyan *et al.*, “Measurement of the Splitting Function in pp and Pb-Pb Collisions at $\sqrt{s_{NN}} = 5.02$ TeV”, *Phys. Rev. Lett.* **120** (2018) 142302, arXiv:1708.09429 [nucl-ex].
- [28] **CMS** Collaboration, A. M. Sirunyan *et al.*, “Measurements of the differential jet cross section as a function of the jet mass in dijet events from proton-proton collisions at $\sqrt{s} = 13$ TeV”, *JHEP* **11** (2018) 113, arXiv:1807.05974 [hep-ex].

- [29] **CMS** Collaboration, A. M. Sirunyan *et al.*, “Jet Shapes of Isolated Photon-Tagged Jets in Pb-Pb and pp Collisions at $\sqrt{s_{NN}} = 5.02$ TeV”, *Phys. Rev. Lett.* **122** (2019) 152001, arXiv:1809.08602 [hep-ex].
- [30] **CMS** Collaboration, A. Tumasyan *et al.*, “Study of quark and gluon jet substructure in Z+jet and dijet events from pp collisions”, *JHEP* **01** (2022) 188, arXiv:2109.03340 [hep-ex].
- [31] **CMS** Collaboration, A. M. Sirunyan *et al.*, “Measurement of b jet shapes in proton-proton collisions at $\sqrt{s} = 5.02$ TeV”, *JHEP* **05** (2021) 054, arXiv:2005.14219 [hep-ex].
- [32] **LHCb** Collaboration, R. Aaij *et al.*, “Study of J/ ψ Production in Jets”, *Phys. Rev. Lett.* **118** (2017) 192001, arXiv:1701.05116 [hep-ex].
- [33] **LHCb** Collaboration, R. Aaij *et al.*, “Measurement of charged hadron production in Z-tagged jets in proton-proton collisions at $\sqrt{s} = 8$ TeV”, *Phys. Rev. Lett.* **123** (2019) 232001, arXiv:1904.08878 [hep-ex].
- [34] **STAR** Collaboration, J. Adam *et al.*, “Measurement of groomed jet substructure observables in p+p collisions at $\sqrt{s} = 200$ GeV with STAR”, *Phys. Lett. B* **811** (2020) 135846, arXiv:2003.02114 [hep-ex].
- [35] **STAR** Collaboration, M. Abdallah *et al.*, “Invariant Jet Mass Measurements in pp Collisions at $\sqrt{s} = 200$ GeV at RHIC”, *Phys. Rev. D* **104** (2021) 052007, arXiv:2103.13286 [hep-ex].
- [36] **STAR** Collaboration, M. S. Abdallah *et al.*, “Differential measurements of jet substructure and partonic energy loss in Au+Au collisions at $\sqrt{s_{NN}} = 200$ GeV”, *Phys. Rev. C* **105** (2022) 044906, arXiv:2109.09793 [nucl-ex].
- [37] M. Connors, C. Nattrass, R. Reed, and S. Salur, “Jet measurements in heavy ion physics”, *Rev. Mod. Phys.* **90** (2018) 025005, arXiv:1705.01974 [nucl-ex].
- [38] **ALICE** Collaboration, S. Acharya *et al.*, “The ALICE experiment: a journey through QCD”, *Eur. Phys. J. C* **84** (2024) 813, arXiv:2211.04384 [nucl-ex].
- [39] J. L. Albacete *et al.*, “Predictions for Cold Nuclear Matter Effects in p+Pb Collisions at $\sqrt{s_{NN}} = 8.16$ TeV”, *Nucl. Phys. A* **972** (2018) 18–85, arXiv:1707.09973 [hep-ph].
- [40] H. Chen, I. Moul, X. Zhang, and H. X. Zhu, “Rethinking jets with energy correlators: Tracks, resummation, and analytic continuation”, *Phys. Rev. D* **102** (2020) 054012, arXiv:2004.11381 [hep-ph].
- [41] P. T. Komiske, I. Moul, J. Thaler, and H. X. Zhu, “Analyzing N-Point Energy Correlators inside Jets with CMS Open Data”, *Phys. Rev. Lett.* **130** (2023) 051901, arXiv:2201.07800 [hep-ph].
- [42] K. Lee, B. Meçaj, and I. Moul, “Conformal Colliders Meet the LHC”, arXiv:2205.03414 [hep-ph].
- [43] C. L. Basham, L. S. Brown, S. D. Ellis, and S. T. Love, “Energy Correlations in Electron - Positron Annihilation: Testing QCD”, *Phys. Rev. Lett.* **41** (1978) 1585.
- [44] **OPAL** Collaboration, P. D. Acton *et al.*, “An improved measurements of $\alpha_s(m_{Z^0})$ using energy correlations with the opal detector at lep”, *Physics Letters B* **276** (1992) 547–564. <https://www.sciencedirect.com/science/article/pii/037026939291681X>.
- [45] **OPAL** Collaboration, P. D. Acton *et al.*, “A Determination of alpha-s (M (Z0)) at LEP using resummed QCD calculations”, *Z. Phys. C* **59** (1993) 1–20.

- [46] A. Kardos, S. Kluth, G. Somogyi, Z. Tulipánt, and A. Verbytskyi, “Precise determination of $\alpha_S(M_Z)$ from a global fit of energy–energy correlation to NNLO+NNLL predictions”, *Eur. Phys. J. C* **78** (2018) 498, arXiv:1804.09146 [hep-ph].
- [47] D. Y. Grigoriev, E. Jankowski, and F. V. Tkachov, “Towards a standard jet definition”, *Phys. Rev. Lett.* **91** (2003) 061801, arXiv:hep-ph/0301185.
- [48] N. A. Sveshnikov and F. V. Tkachov, “Jets and quantum field theory”, *Phys. Lett. B* **382** (1996) 403–408, arXiv:hep-ph/9512370.
- [49] D. Y. Grigoriev, E. Jankowski, and F. V. Tkachov, “Optimal jet finder”, *Comput. Phys. Commun.* **155** (2003) 42–64, arXiv:hep-ph/0301226.
- [50] F. V. Tkachov, “A Theory of jet definition”, *Int. J. Mod. Phys. A* **17** (2002) 2783–2884, arXiv:hep-ph/9901444.
- [51] D. Neill, G. Vita, I. Vitev, and H. X. Zhu, “Energy-Energy Correlators for Precision QCD”, in *Snowmass 2021*. 3, 2022. arXiv:2203.07113 [hep-ph].
- [52] H. Chen, M. Jaarsma, Y. Li, I. Moul, W. J. Waalewijn, and H. X. Zhu, “Multi-collinear splitting kernels for track function evolution”, *JHEP* **07** (2023) 185, arXiv:2210.10058 [hep-ph].
- [53] H. Chen, M. Jaarsma, Y. Li, I. Moul, W. J. Waalewijn, and H. X. Zhu, “Collinear Parton Dynamics Beyond DGLAP”, arXiv:2210.10061 [hep-ph].
- [54] M. Jaarsma, Y. Li, I. Moul, W. Waalewijn, and H. X. Zhu, “Renormalization group flows for track function moments”, *JHEP* **06** (2022) 139, arXiv:2201.05166 [hep-ph].
- [55] Y. Li, I. Moul, S. S. van Velzen, W. J. Waalewijn, and H. X. Zhu, “Extending Precision Perturbative QCD with Track Functions”, *Phys. Rev. Lett.* **128** (2022) 182001, arXiv:2108.01674 [hep-ph].
- [56] CMS Collaboration, A. Hayrapetyan *et al.*, “Measurement of Energy Correlators inside Jets and Determination of the Strong Coupling $\alpha_S(m_Z)$ ”, *Phys. Rev. Lett.* **133** (2024) 071903, arXiv:2402.13864 [hep-ex].
- [57] ALICE Collaboration, E. Abbas *et al.*, “Performance of the ALICE VZERO system”, *JINST* **8** (2013) P10016, arXiv:1306.3130 [nucl-ex].
- [58] ALICE Collaboration, S. Acharya *et al.*, “ALICE 2017 luminosity determination for pp collisions at $\sqrt{s} = 5$ TeV”, ALICE-PUBLIC-2018-014. <https://cds.cern.ch/record/2648933>.
- [59] ALICE Collaboration, K. Aamodt *et al.*, “Alignment of the ALICE Inner Tracking System with cosmic-ray tracks”, *JINST* **5** (2010) P03003, arXiv:1001.0502 [physics.ins-det].
- [60] J. Alme *et al.*, “The ALICE TPC, a large 3-dimensional tracking device with fast readout for ultra-high multiplicity events”, *Nucl. Instrum. Meth. A* **622** (2010) 316–367, arXiv:1001.1950 [physics.ins-det].
- [61] ALICE Collaboration, B. B. Abelev *et al.*, “Performance of the ALICE Experiment at the CERN LHC”, *Int. J. Mod. Phys. A* **29** (2014) 1430044, arXiv:1402.4476 [nucl-ex].
- [62] ALICE Collaboration, K. Aamodt *et al.*, “The ALICE experiment at the CERN LHC”, *JINST* **3** (2008) S08002.
- [63] ALICE Collaboration, B. Abelev *et al.*, “Measurement of charged jet suppression in Pb-Pb collisions at $\sqrt{s_{NN}} = 2.76$ TeV”, *JHEP* **03** (2014) 013, arXiv:1311.0633 [nucl-ex].

- [64] M. Cacciari, G. P. Salam, and G. Soyez, “FastJet User Manual”, *Eur. Phys. J. C* **72** (2012) 1896, arXiv:1111.6097 [hep-ph].
- [65] T. Sjöstrand *et al.*, “An introduction to PYTHIA 8.2”, *Comput. Phys. Commun.* **191** (2015) 159–177, arXiv:1410.3012 [hep-ph].
- [66] P. Skands, S. Carrazza, and J. Rojo, “Tuning PYTHIA 8.1: the Monash 2013 Tune”, *Eur. Phys. J. C* **74** (2014) 3024, arXiv:1404.5630 [hep-ph].
- [67] R. Brun, F. Bruyant, M. Maire, A. C. McPherson, and P. Zancarini, *GEANT 3: user’s guide Geant 3.10, Geant 3.11; rev. version*. CERN, Geneva, Sep, 1987. <https://cds.cern.ch/record/1119728>.
- [68] ALICE Collaboration, S. Acharya *et al.*, “Azimuthally-differential pion femtoscopy relative to the third harmonic event plane in Pb-Pb collisions at $\sqrt{s_{NN}} = 2.76$ TeV”, *Phys. Lett. B* **785** (2018) 320–331, arXiv:1803.10594 [nucl-ex].
- [69] G. D’Agostini, “A multidimensional unfolding method based on Bayes’ theorem”, *Nucl. Instrum. Meth. A* **362** (1994) 487 – 498.
- [70] T. Auye, “Unfolding algorithms and tests using RooUnfold”, in *PHYSTAT 2011*, pp. 313–318. CERN, Geneva, 2011. arXiv:1105.1160 [physics.data-an].
- [71] ALICE Collaboration, S. Acharya *et al.*, “Measurement of charged jet cross section in pp collisions at $\sqrt{s} = 5.02$ TeV”, *Phys. Rev. D* **100** (2019) 092004, arXiv:1905.02536 [nucl-ex].
- [72] J. Bellm *et al.*, “Herwig 7.0/Herwig++ 3.0 release note”, *Eur. Phys. J. C* **76** (Apr, 2016) 196, arXiv:1512.01178 [hep-ph].
- [73] Y. L. Dokshitzer, G. Marchesini, and B. R. Webber, “Non-perturbative effects in the energy energy correlation”, *JHEP* **07** (1999) 012, arXiv:hep-ph/9905339.
- [74] G. P. Korchemsky and G. F. Sterman, “Power corrections to event shapes and factorization”, *Nucl. Phys. B* **555** (1999) 335–351, arXiv:hep-ph/9902341.
- [75] S. T. Schindler, I. W. Stewart, and Z. Sun, “Renormalons in the energy-energy correlator”, *JHEP* **10** (2023) 187, arXiv:2305.19311 [hep-ph].
- [76] K. Lee, A. Pathak, I. Stewart, and Z. Sun, “Nonperturbative Effects in Energy Correlators: From Characterizing Confinement Transition to Improving α_s Extraction”, arXiv:2405.19396 [hep-ph].
- [77] P. Skands, S. Carrazza, and J. Rojo, “Tuning PYTHIA 8.1: the Monash 2013 tune”, *Eur. Phys. J. C* **74** (Aug, 2014) 3024, arXiv:1404.5630 [hep-ph].
- [78] Sherpa Collaboration, E. Bothmann *et al.*, “Event Generation with Sherpa 2.2”, *SciPost Phys.* **7** (2019) 034, arXiv:1905.09127 [hep-ph].
- [79] W. A. de Jong, K. Lee, J. Mulligan, M. Płoskoń, F. Ringer, and X. Yao, “Quantum simulation of nonequilibrium dynamics and thermalization in the Schwinger model”, *Phys. Rev. D* **106** (2022) 054508, arXiv:2106.08394 [quant-ph].
- [80] F. V. Tkachov, “Measuring multi - jet structure of hadronic energy flow or What is a jet?”, *Int. J. Mod. Phys. A* **12** (1997) 5411–5529, arXiv:hep-ph/9601308.

A Characterization of the transition region

To quantitatively characterize the transition region, a fit is performed to extract the transition peak position and peak height as shown below in Fig. A.1. The fit function used is log-normal function:

$$\text{Gaus}(\ln(R_L)) = C \cdot \exp\left(-\frac{(\ln R_L - \mu)^2}{2\sigma^2}\right) \quad (\text{A.1})$$

where C is a constant factor. The fit range is limited to R_L range within $\mu \pm 0.7\sigma$ where the fit agrees with EEC distributions reasonably. The fit results and uncertainties are shown in Fig. A.1. R_L^{peak} and its uncertainty is extracted via $R_L^{\text{peak}} = \exp(\mu)$.

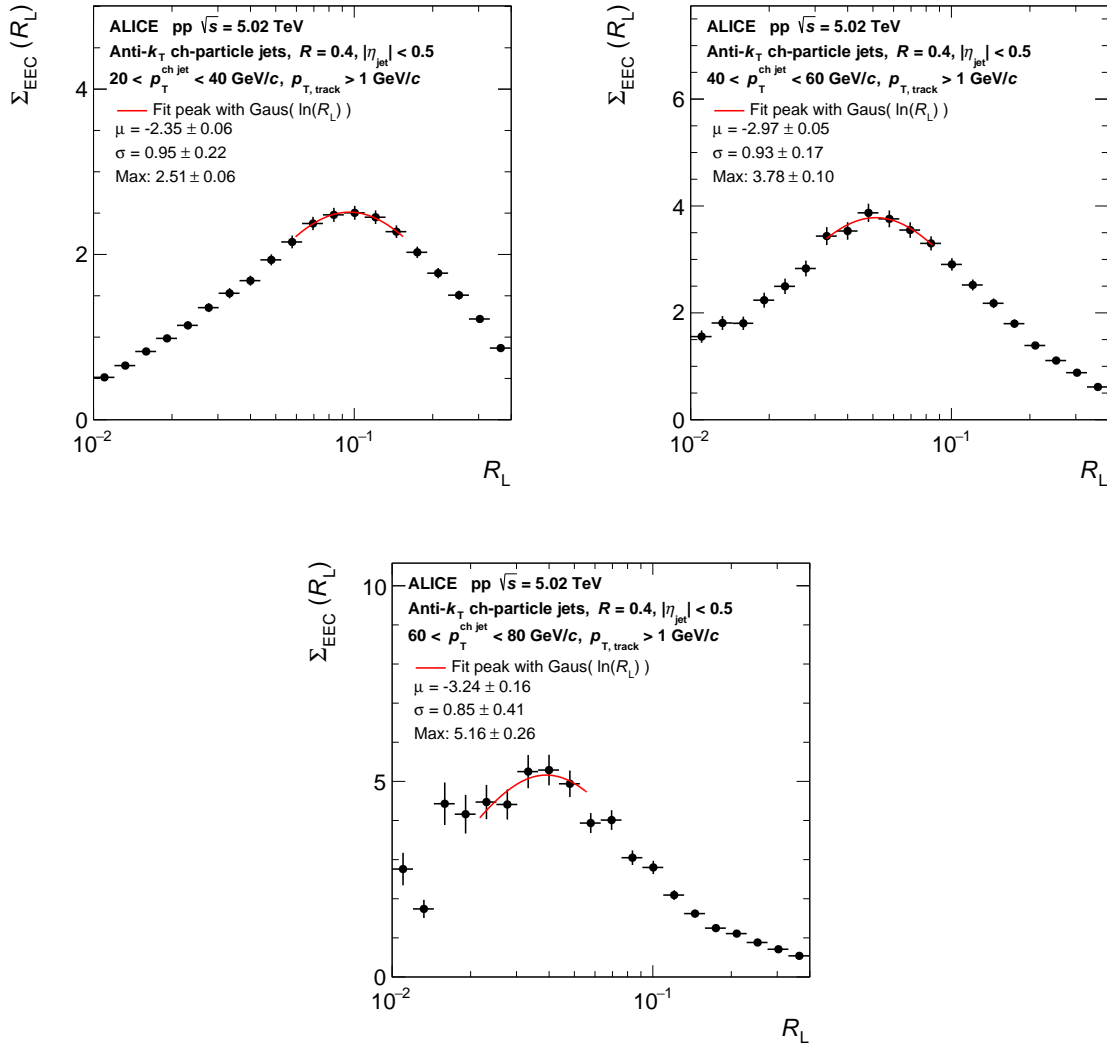


Figure A.1: Extraction of the peak position and height of the EEC distributions in different jet p_T ranges. The fit function and fitting range used is shown by the red curve.

With the extracted values from Fig. A.1, the jet p_T dependence of the peak position and peak height are examined in Fig. A.2, where we can see that:

$$R_L^{\text{peak}} \times \langle p_T^{\text{ch jet}} \rangle \approx 2.42 \pm 0.17 \text{ GeV}/c \quad (\text{A.2})$$

$$\Sigma_{\text{EEC}}^{\text{peak}} \times \ln \langle p_T^{\text{ch jet}} \rangle / \langle p_T^{\text{ch jet}} \rangle \approx 0.32 \pm 0.01 (\text{GeV}/c)^{-1} \quad (\text{A.3})$$

where $\langle p_T^{\text{ch jet}} \rangle$ for the three jet $p_T^{\text{ch jet}}$ intervals (20–40, 40–60, 60–80 GeV/c) are 25.1, 46.7, 67.5 GeV/c. $\ln\langle p_T^{\text{ch jet}} \rangle$ represents $\ln(\langle p_T^{\text{ch jet}} \rangle / (\text{GeV}/c))$ as explained in footnote 2.

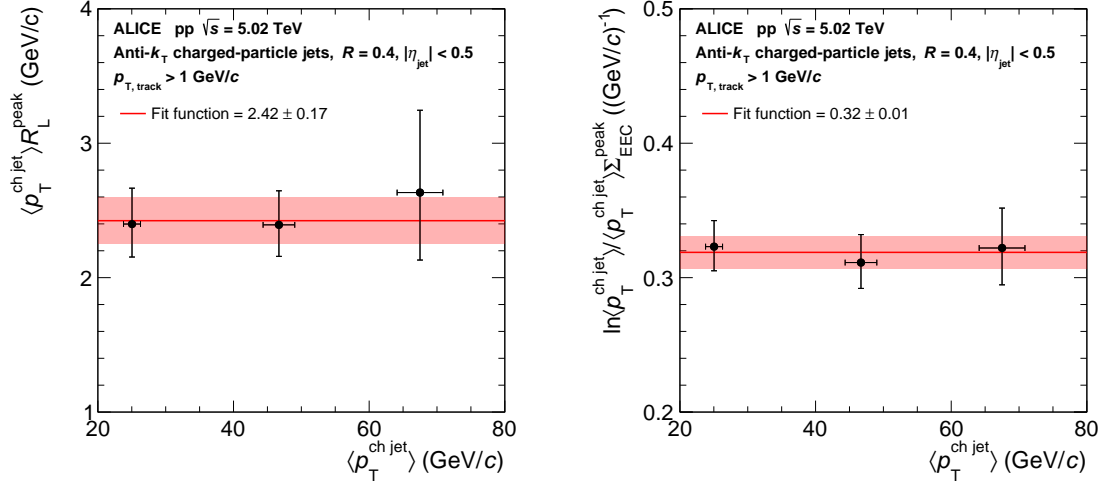


Figure A.2: Left: the jet p_T dependence of the transition peak position R_L^{peak} . Right: the jet p_T dependence of the transition peak height $\Sigma_{\text{EEC}}^{\text{peak}}$. $\ln\langle p_T^{\text{ch jet}} \rangle$ in the y-axis represents $\ln(\langle p_T^{\text{ch jet}} \rangle / (\text{GeV}/c))$ as explained in footnote 2.

The jet p_T dependence of the transition region described in Eq.A.2 and A.3 can also be viewed in Fig. 2.

B Results with different track threshold selections

The reported results in the main text use charged-particle tracks with $p_{T,\text{track}} > 1$ GeV/c threshold cut when constructing the EECs. We also carried out the measurement with lower threshold cuts, $p_{T,\text{track}} > 0.15$ GeV/c and $p_{T,\text{track}} > 0.5$ GeV/c. The comparison of the EEC distributions with different track threshold selections is shown in Fig. B.1. Different track threshold selections lead to a small difference in the EEC distributions at large R_L and the difference becomes negligible for jets with higher p_T . The transition peak positions are not affected by the different $p_{T,\text{track}}$ selections used.

C PYTHIA 8 studies

To obtain more intuition about the transition region in the EEC distributions and the hadronization process, we studied with PYTHIA 8 (8.235 version) Monash tune how different parameters impact the EECs. The parameters checked are the following:

- Parameter related to the hadron fragmentation: StringPT:sigma, which corresponds to the average transverse momentum from string breaking.
- Parameter related to the parton shower: TimeShower:pTmin, which corresponds to the parton shower cut-off p_T for QCD emissions.

We then vary the above parameters up and down by 30% from the default values and compare how it impacts the EEC cross section as function of R_L . We looked both at the charged hadron level and parton level to gain further insight into the impact at different stages of the jet evolution modeled by PYTHIA 8. The results are shown in Fig. C.1 and Fig. C.2. The blue markers always correspond to the default PYTHIA 8 tuning in Monash tune.

From Fig. C.1, it can be seen that the TimeShower:pTmin parameter has a significant impact on the EECs at the parton level but shows almost no visible impact on the EEC at the charged hadron level.

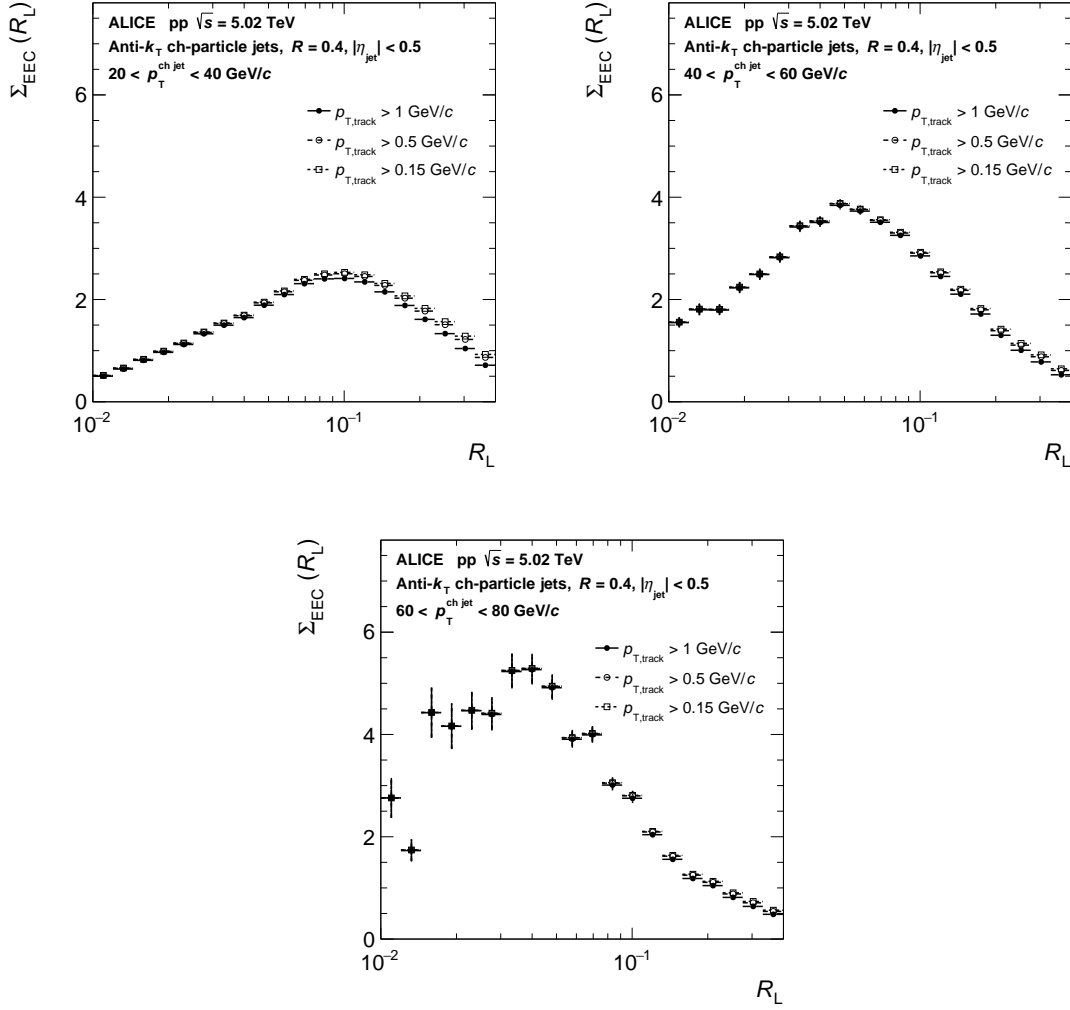


Figure B.1: Comparison Σ_{EEC} as a function of R_L with 0.15 GeV/c, 0.5 GeV/c, and 1 GeV/c track p_T threshold cut in the $p_T^{\text{ch,jet}}$ intervals 20–40, 40–60, and 60–80 GeV/c. Systematic uncertainties are not shown here.

Such an observation indicates that the transition peak of the hadron level EEC (what can be measured) is not very sensitive to the QCD shower cutoff parameter. Despite not being able to measure the parton level EEC, it is interesting to see that there is a turnover transition region and the location of that moves to a smaller angle when changing the QCD shower cutoff to a smaller value, while the transition location moves towards a larger angle with increasing QCD shower cutoff. This is consistent with the intuition that the R_L is related to the energy scale of the parton splitting, hence when we lower the shower cutoff, the EEC continues on the parton shower trend for a wider R_L region. Once the hadronization effects are included, the transition region with different TimeShower:pTmin appear at a very similar location.

Contrary to the observation in Fig. C.1, in Fig. C.2 we observe that when we alter StringPT:sigma, which is directly related to the hadronization process, a significant change is observed in the EECs at hadron level but no visible difference at the parton level. Since StringPT:sigma is only related to the hadron fragmentation, it makes sense that the variation of this parameter does not affect the EECs at parton level. On the other hand, at the hadron level, the transition peak seems to be sensitive to the variations of StringPT:sigma. The transition location shifts to smaller angles when we decrease this parameter. The smaller StringPT:sigma corresponds to smaller string tension where the Lund strings break up later and a lower energy scale. This picture is consistent with the observed shift when StringPT:sigma is decreased.

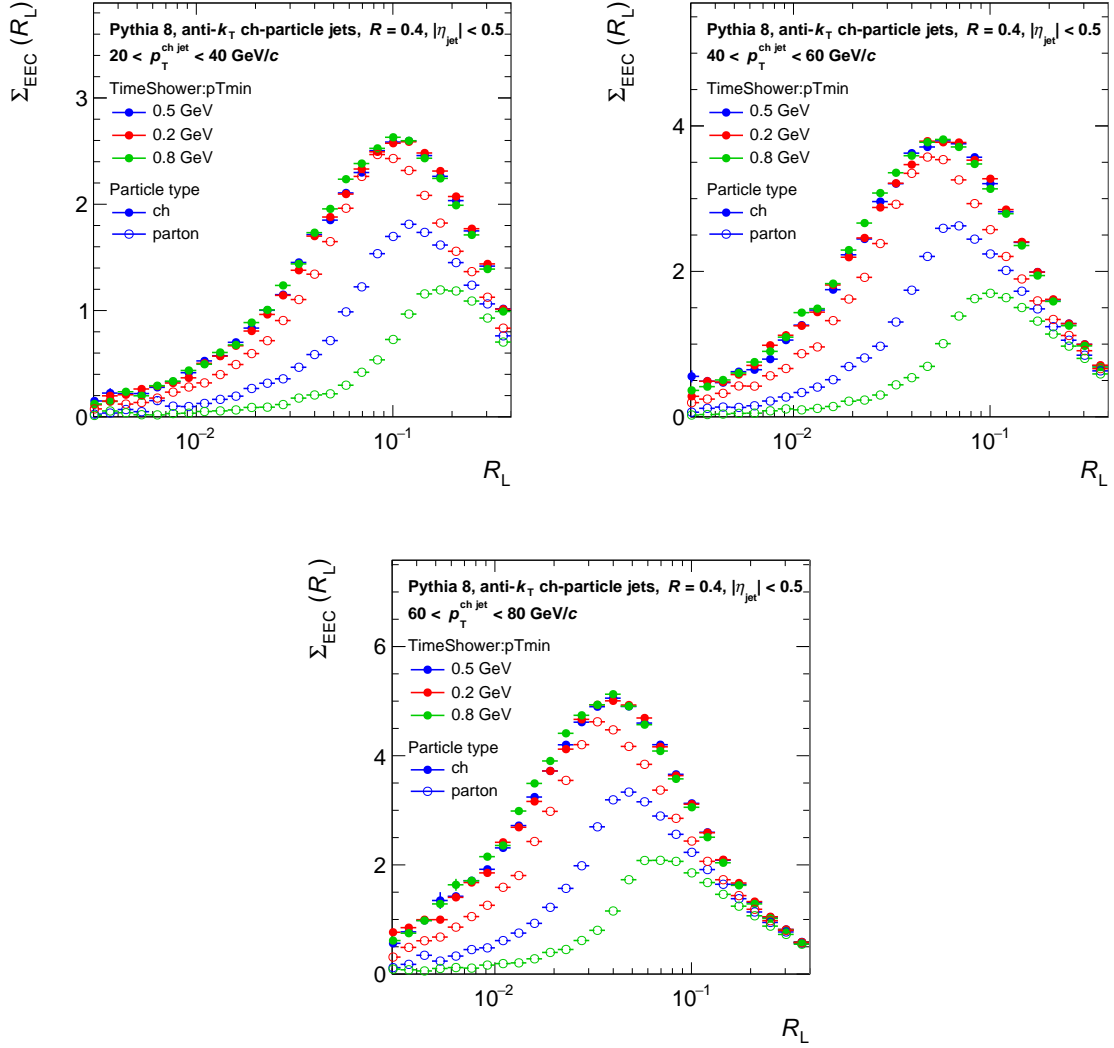


Figure C.1: Comparison of Σ_{EEC} as a function of R_L with different values for TimeShower:pTmin using generated Pythia events. The default setting is 0.5 (blue markers). The parton level distributions are made from parton jets that are matched to the charged jets with p_T range indicated in each figure.

These PYTHIA 8 studies support that the transition peak is sensitive to hadronization process. We hope these studies and the reported measurement can motivate first principle calculations which can help draw conclusive statements.

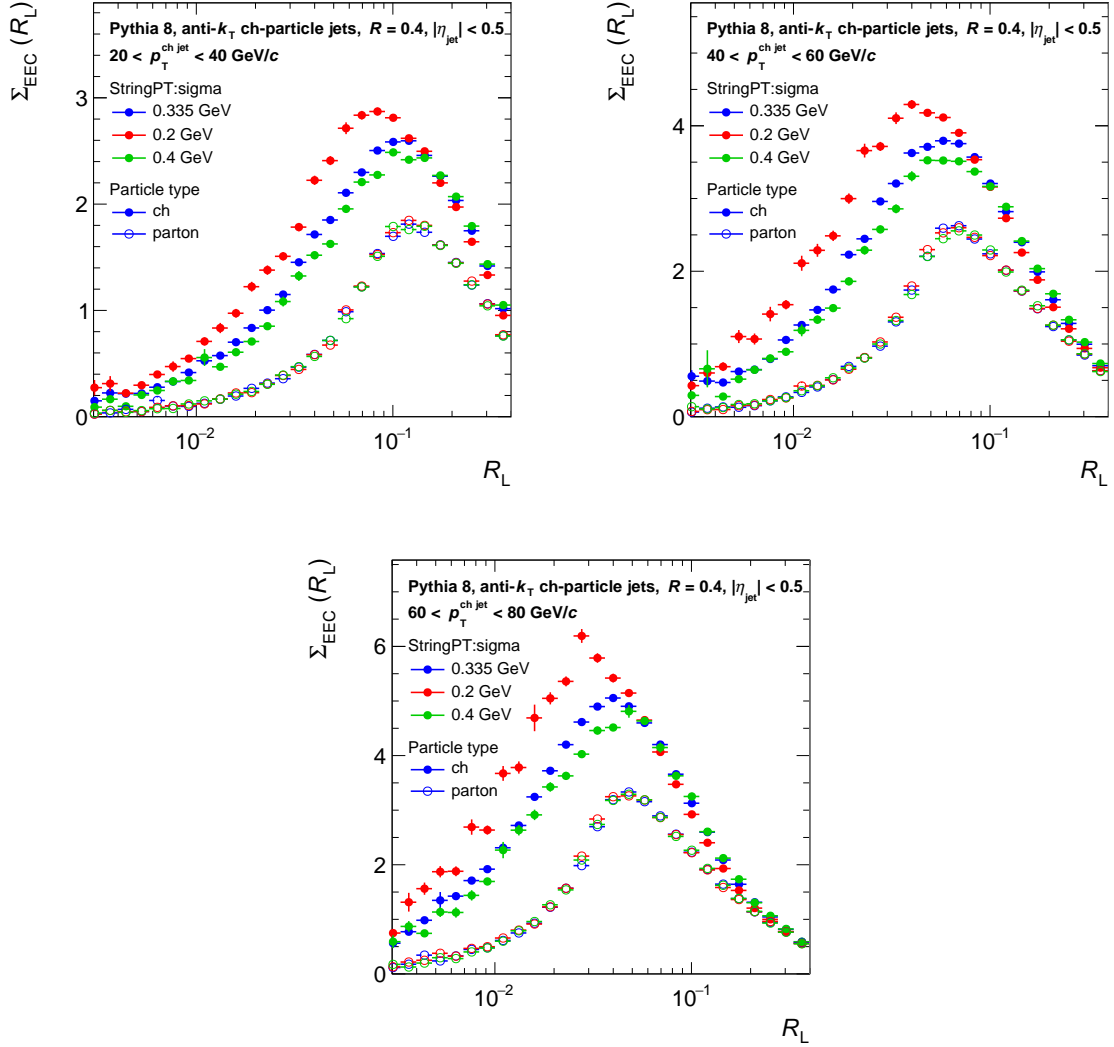


Figure C.2: Comparison of Σ_{EEC} section as a function of R_L with different values for StringPT:sigma using generated PYTHIA 8 events. The default setting is 0.335 (blue markers). The parton level distributions are made from parton jets that are matched to the charged jets with p_T range indicated in each figure.

D The ALICE Collaboration

S. Acharya ¹²⁶, A. Agarwal¹³⁴, G. Aglieri Rinella ³², L. Aglietta ²⁴, M. Agnello ²⁹, N. Agrawal ²⁵, Z. Ahammed ¹³⁴, S. Ahmad ¹⁵, S.U. Ahn ⁷¹, I. Ahuja ³⁷, A. Akindinov ¹⁴⁰, V. Akishina³⁸, M. Al-Turany ⁹⁶, D. Aleksandrov ¹⁴⁰, B. Alessandro ⁵⁶, H.M. Alfanda ⁶, R. Alfaro Molina ⁶⁷, B. Ali ¹⁵, A. Alici ²⁵, N. Alizadehvandchali ¹¹⁵, A. Alkin ¹⁰³, J. Alme ²⁰, G. Alocco ^{24,52}, T. Alt ⁶⁴, A.R. Altamura ⁵⁰, I. Altsybeev ⁹⁴, J.R. Alvarado ⁴⁴, C.O.R. Alvarez⁴⁴, M.N. Anaam ⁶, C. Andrei ⁴⁵, N. Andreou ¹¹⁴, A. Andronic ¹²⁵, E. Andronov ¹⁴⁰, V. Angelov ⁹³, F. Antinori ⁵⁴, P. Antonioli ⁵¹, N. Apadula ⁷³, L. Aphecetche ¹⁰², H. Appelshäuser ⁶⁴, C. Arata ⁷², S. Arcelli ²⁵, R. Arnaldi ⁵⁶, J.G.M.C.A. Arneiro ¹⁰⁹, I.C. Arsene ¹⁹, M. Arslanodk ¹³⁷, A. Augustinus ³², R. Averbeck ⁹⁶, D. Averyanov ¹⁴⁰, M.D. Azmi ¹⁵, H. Baba¹²³, A. Badalà ⁵³, J. Bae ¹⁰³, Y. Bae¹⁰³, Y.W. Baek

⁴⁰, X. Bai ¹¹⁹, R. Bailhache ⁶⁴, Y. Bailung ⁴⁸, R. Bala ⁹⁰, A. Balbino ²⁹, A. Baldisseri ¹²⁹, B. Balis ², Z. Banoo ⁹⁰, V. Barbasova³⁷, F. Barile ³¹, L. Barioglio ⁵⁶, M. Barlou⁷⁷, B. Barman⁴¹, G.G. Barnaföldi ⁴⁶, L.S. Barnby ¹¹⁴, E. Barreau ¹⁰², V. Barret ¹²⁶, L. Barreto ¹⁰⁹, C. Bartels ¹¹⁸, K. Barth ³², E. Bartsch ⁶⁴, N. Bastid ¹²⁶, S. Basu ⁷⁴, G. Batigne ¹⁰², D. Battistini ⁹⁴, B. Batyunya ¹⁴¹, D. Bauri⁴⁷, J.L. Bazo Alba ¹⁰⁰, I.G. Bearden ⁸², C. Beattie ¹³⁷, P. Becht ⁹⁶, D. Behera ⁴⁸, I. Belikov ¹²⁸, A.D.C. Bell Hechavarria ¹²⁵, F. Bellini ²⁵, R. Bellwied ¹¹⁵, S. Belokurova ¹⁴⁰, L.G.E. Beltran ¹⁰⁸, Y.A.V. Beltran ⁴⁴, G. Bencedi ⁴⁶, A. Bensaoula¹¹⁵, S. Beole ²⁴, Y. Berdnikov ¹⁴⁰, A. Berdnikova ⁹³, L. Bergmann ⁹³, M.G. Besoiu ⁶³, L. Betev ³², P.P. Bhaduri ¹³⁴, A. Bhasin ⁹⁰, B. Bhattacharjee ⁴¹, L. Bianchi ²⁴, J. Bielčik ³⁵, J. Bielčíková ⁸⁵, A.P. Bigot

¹²⁸, A. Bilandzic ⁹⁴, G. Biro ⁴⁶, S. Biswas ⁴, N. Bize ¹⁰², J.T. Blair ¹⁰⁷, D. Blau ¹⁴⁰, M.B. Blidaru ⁹⁶, N. Bluhme³⁸, C. Blume ⁶⁴, F. Bock ⁸⁶, T. Bodova ²⁰, J. Bok ¹⁶, L. Boldizsár ⁴⁶, M. Bombara ³⁷, P.M. Bond ³², G. Bonomi ^{133,55}, H. Borel ¹²⁹, A. Borissov ¹⁴⁰, A.G. Borquez Carcamo ⁹³, E. Botta ²⁴, Y.E.M. Bouziani ⁶⁴, L. Bratrud ⁶⁴, P. Braun-Munzinger ⁹⁶, M. Bregant ¹⁰⁹, M. Broz ³⁵, G.E. Bruno ^{95,31}, V.D. Buchakchiev ³⁶, M.D. Buckland ⁸⁴, D. Budnikov ¹⁴⁰, H. Buesching ⁶⁴, S. Bufalino ²⁹, P. Buhler ¹⁰¹, N. Burmasov ¹⁴⁰, Z. Buthelezi ^{68,122}, A. Bylinkin ²⁰, S.A. Bysiak¹⁰⁶, J.C. Cabanillas Noris ¹⁰⁸, M.F.T. Cabrera¹¹⁵, H. Caines ¹³⁷, A. Caliva ²⁸, E. Calvo Villar ¹⁰⁰, J.M.M. Camacho ¹⁰⁸, P. Camerini ²³, F.D.M. Canedo ¹⁰⁹, S.L. Cantway ¹³⁷, M. Carabas ¹¹², A.A. Carballo ³², F. Carnesecchi ³², R. Caron ¹²⁷, L.A.D. Carvalho ¹⁰⁹, J. Castillo Castellanos ¹²⁹, M. Castoldi

³², F. Catalano ³², S. Cattaruzzi ²³, R. Cerri ²⁴, I. Chakaberia ⁷³, P. Chakraborty ¹³⁵, S. Chandra ¹³⁴, S. Chapeland ³², M. Chartier ¹¹⁸, S. Chattopadhyay¹³⁴, M. Chen³⁹, T. Cheng ⁶, C. Cheshkov ¹²⁷, D. Chiappara²⁷, V. Chibante Barroso ³², D.D. Chinellato ¹⁰¹, E.S. Chizzali ^{11,94}, J. Cho ⁵⁸, S. Cho ⁵⁸, P. Chochula ³², Z.A. Chochulska¹³⁵, D. Choudhury⁴¹, S. Choudhury⁹⁸, P. Christakoglou ⁸³, C.H. Christensen ⁸², P. Christiansen ⁷⁴, T. Chujo ¹²⁴, M. Ciacco ²⁹, C. Cicalo ⁵², F. Cindolo ⁵¹, M.R. Ciupek⁹⁶, G. Clai^{III,51}, F. Colamaria ⁵⁰, J.S. Colburn⁹⁹, D. Colella ³¹, A. Colelli³¹, M. Colocci ²⁵, M. Concas ³², G. Conesa Balbastre ⁷², Z. Conesa del Valle ¹³⁰, G. Contin ²³, J.G. Contreras ³⁵, M.L. Coquet ¹⁰², P. Cortese ^{132,56}, M.R. Cosentino ¹¹¹, F. Costa ³², S. Costanza ^{21,55}, C. Cot ¹³⁰, P. Crochet ¹²⁶, M.M. Czarnynoga¹³⁵, A. Dainese ⁵⁴, G. Dange³⁸, M.C. Danisch ⁹³, A. Danu ⁶³, P. Das ^{32,79}, S. Das ⁴, A.R. Dash ¹²⁵, S. Dash ⁴⁷, A. De Caro ²⁸, G. de Cataldo ⁵⁰, J. de Cuveland³⁸, A. De Falco

²², D. De Gruttola ²⁸, N. De Marco ⁵⁶, C. De Martin ²³, S. De Pasquale ²⁸, R. Deb ¹³³, R. Del Grande ⁹⁴, L. Dello Stritto ³², W. Deng ⁶, K.C. Devereaux¹⁸, P. Dhankher ¹⁸, D. Di Bari ³¹, A. Di Mauro ³², B. Di Ruzza ¹³¹, B. Diab ¹²⁹, R.A. Diaz ^{141,7}, Y. Ding ⁶, J. Ditzel ⁶⁴, R. Divià ³², Ø. Djuvsland²⁰, U. Dmitrieva ¹⁴⁰, A. Dobrin ⁶³, B. Dönigus ⁶⁴, J.M. Dubinski ¹³⁵, A. Dubla ⁹⁶, P. Dupieux ¹²⁶, N. Dzalaiova¹³, T.M. Eder ¹²⁵, R.J. Ehlers ⁷³, F. Eisenhut ⁶⁴, R. Ejima ⁹¹, D. Elia ⁵⁰, B. Erazmus ¹⁰², F. Ercolessi ²⁵, B. Espagnon ¹³⁰, G. Eulisse ³², D. Evans ⁹⁹, S. Evdokimov ¹⁴⁰, L. Fabbietti ⁹⁴, M. Faggin ²³, J. Faivre ⁷², F. Fan ⁶, W. Fan ⁷³, A. Fantoni ⁴⁹, M. Fasel ⁸⁶, G. Feofilov ¹⁴⁰, A. Fernández Téllez ⁴⁴, L. Ferrandi ¹⁰⁹, M.B. Ferrer ³², A. Ferrero ¹²⁹, C. Ferrero ^{IV,56}, A. Ferretti ²⁴, V.J.G. Feuillard

⁹³, V. Filova ³⁵, D. Finogeev ¹⁴⁰, F.M. Fionda ⁵², E. Flatland³², F. Flor ^{137,115}, A.N. Flores ¹⁰⁷, S. Foertsch ⁶⁸, I. Fokin ⁹³, S. Fokin ¹⁴⁰, U. Follo ^{IV,56}, E. Fragiaco ⁵⁷, E. Frajna ⁴⁶, U. Fuchs ³², N. Funicello ²⁸, C. Furget ⁷², A. Furs ¹⁴⁰, T. Fusayasu ⁹⁷, J.J. Gaardhøje ⁸², M. Gagliardi ²⁴, A.M. Gago ¹⁰⁰, T. Gahlaut⁴⁷, C.D. Galvan ¹⁰⁸, S. Gami⁷⁹, D.R. Gangadharan ¹¹⁵, P. Ganoti ⁷⁷, C. Garabatos ⁹⁶, J.M. Garcia⁴⁴, T. García Chávez ⁴⁴, E. Garcia-Solis ⁹, C. Gargiulo ³², P. Gasik ⁹⁶, H.M. Gaur³⁸, A. Gautam ¹¹⁷, M.B. Gay Ducati ⁶⁶, M. Germain ¹⁰², R.A. Gernhaeuser⁹⁴, C. Ghosh¹³⁴, M. Giacalone ⁵¹, G. Gioachin ²⁹, S.K. Giri¹³⁴, P. Giubellino ^{96,56}, P. Giubilato ²⁷, A.M.C. Glaenger ¹²⁹, P. Glässel ⁹³, E. Glimos ¹²¹, D.J.Q. Goh⁷⁵, V. Gonzalez ¹³⁶, P. Gordeev ¹⁴⁰, M. Gorgon ², K. Goswami ⁴⁸, S. Gotovac³³, V. Grabski ⁶⁷, L.K. Graczykowski ¹³⁵, E. Grecka ⁸⁵, A. Grelli ⁵⁹, C. Grigoras ³², V. Grigoriev ¹⁴⁰, S. Grigoryan

F. Grosa ³², J.F. Grosse-Oetringhaus ³², R. Grosso ⁹⁶, D. Grund ³⁵, N.A. Grunwald⁹³, G.G. Guardiano ¹¹⁰, R. Guernane ⁷², M. Guilbaud ¹⁰², K. Gulbrandsen ⁸², J.J.W.K. Gumprecht¹⁰¹, T. Gündem ⁶⁴, T. Gunji ¹²³, W. Guo ⁶, A. Gupta ⁹⁰, R. Gupta ⁹⁰, R. Gupta ⁴⁸, K. Gwizdziel ¹³⁵, L. Gyulai ⁴⁶, C. Hadjidakis ¹³⁰, F.U. Haider ⁹⁰, S. Haidlova ³⁵, M. Haldar⁴, H. Hamagaki ⁷⁵, Y. Han ¹³⁹, B.G. Hanley ¹³⁶, R. Hannigan ¹⁰⁷, J. Hansen ⁷⁴, M.R. Haque ⁹⁶, J.W. Harris ¹³⁷, A. Harton ⁹, M.V. Hartung ⁶⁴, H. Hassan ¹¹⁶, D. Hatzifotiadou ⁵¹, P. Hauer ⁴², L.B. Havener ¹³⁷, E. Hellbär ³², H. Helstrup ³⁴, M. Hemmer ⁶⁴, T. Herman ³⁵, S.G. Hernandez¹¹⁵, G. Herrera Corral ⁸, S. Herrmann ¹²⁷, K.F. Hetland ³⁴, B. Heybeck ⁶⁴, H. Hillemanns ³², B. Hippolyte ¹²⁸, I.P.M. Hobus⁸³, F.W. Hoffmann ⁷⁰, B. Hofman ⁵⁹, M. Horst ⁹⁴, A. Horzyk ², Y. Hou ⁶, P. Hristov ³², P. Huhn⁶⁴, L.M. Huhta ¹¹⁶, T.J. Humanic ⁸⁷, A. Hutson ¹¹⁵, D. Hutter ³⁸, M.C. Hwang ¹⁸, R. Ilkaev¹⁴⁰, M. Inaba ¹²⁴, G.M. Innocenti ³², M. Ippolitov ¹⁴⁰, A. Isakov ⁸³, T. Isidori ¹¹⁷, M.S. Islam ^{47,98}, S. Iurchenko¹⁴⁰, M. Ivanov¹³, M. Ivanov ⁹⁶, V. Ivanov ¹⁴⁰, K.E. Iversen ⁷⁴, M. Jablonski ², B. Jacak ^{18,73}, N. Jacazio ²⁵, P.M. Jacobs ⁷³, S. Jadlovská¹⁰⁵, J. Jadlovsky¹⁰⁵, S. Jaelani ⁸¹, C. Jahnke ¹⁰⁹, M.J. Jakubowska ¹³⁵, M.A. Janik ¹³⁵, T. Janson⁷⁰, S. Ji ¹⁶, S. Jia ¹⁰, T. Jiang ¹⁰, A.A.P. Jimenez ⁶⁵, F. Jonas ⁷³, D.M. Jones ¹¹⁸, J.M. Jowett ^{32,96}, J. Jung ⁶⁴, M. Jung ⁶⁴, A. Junique ³², A. Jusko ⁹⁹, J. Kaewjai¹⁰⁴, P. Kalinak ⁶⁰, A. Kalweit ³², A. Karasu Uysal ^{V,138}, D. Karatovic ⁸⁸, N. Karatzenis⁹⁹, O. Karavichev ¹⁴⁰, T. Karavicheva ¹⁴⁰, E. Karpechev ¹⁴⁰, M.J. Karwowska ¹³⁵, U. Kebschull ⁷⁰, M. Keil ³², B. Ketzer ⁴², J. Keul ⁶⁴, S.S. Khade ⁴⁸, A.M. Khan ¹¹⁹, S. Khan ¹⁵, A. Khanzadeev ¹⁴⁰, Y. Kharlov ¹⁴⁰, A. Khatun ¹¹⁷, A. Khuntia ³⁵, Z. Khuranova ⁶⁴, B. Kileng ³⁴, B. Kim ¹⁰³, C. Kim ¹⁶, D.J. Kim ¹¹⁶, D. Kim¹⁰³, E.J. Kim ⁶⁹, J. Kim ¹³⁹, J. Kim ⁵⁸, J. Kim ^{32,69}, M. Kim ¹⁸, S. Kim ¹⁷, T. Kim ¹³⁹, K. Kimura ⁹¹, A. Kirkova³⁶, S. Kirsch ⁶⁴, I. Kisel ³⁸, S. Kiselev ¹⁴⁰, A. Kisiel ¹³⁵, J.L. Klay ⁵, J. Klein ³², S. Klein ⁷³, C. Klein-Bösing ¹²⁵, M. Kleiner ⁶⁴, T. Klemenz ⁹⁴, A. Kluge ³², C. Kobdaj ¹⁰⁴, R. Kohara¹²³, T. Kollegger⁹⁶, A. Kondratyev ¹⁴¹, N. Kondratyeva ¹⁴⁰, J. König ⁶⁴, S.A. Königstorfer ⁹⁴, P.J. Konopka ³², G. Kornakov ¹³⁵, M. Korwieser ⁹⁴, S.D. Koryciak ², C. Koster⁸³, A. Kotliarov ⁸⁵, N. Kovacic⁸⁸, V. Kovalenko ¹⁴⁰, M. Kowalski ¹⁰⁶, V. Kozuharov ³⁶, G. Kozlov³⁸, I. Králik ⁶⁰, A. Kravčáková ³⁷, L. Krcal ^{32,38}, M. Krivda ^{99,60}, F. Krizek ⁸⁵, K. Krizkova Gajdosova ³², C. Krug ⁶⁶, M. Krüger ⁶⁴, D.M. Krupova ³⁵, E. Kryshen ¹⁴⁰, V. Kučera ⁵⁸, C. Kuhn ¹²⁸, P.G. Kuijjer ⁸³, T. Kumaoka¹²⁴, D. Kumar¹³⁴, L. Kumar ⁸⁹, N. Kumar⁸⁹, S. Kumar ⁵⁰, S. Kundu ³², P. Kurashvili ⁷⁸, A.B. Kurepin ¹⁴⁰, A. Kuryakin ¹⁴⁰, S. Kushpil ⁸⁵, V. Kuskov ¹⁴⁰, M. Kutyla¹³⁵, A. Kuznetsov¹⁴¹, M.J. Kweon ⁵⁸, Y. Kwon ¹³⁹, S.L. La Pointe ³⁸, P. La Rocca ²⁶, A. Lakrathok¹⁰⁴, M. Lamanna ³², A.R. Landou ⁷², R. Langoy ¹²⁰, P. Larionov ³², E. Laudi ³², L. Lautner ⁹⁴, R.A.N. Laveaga¹⁰⁸, R. Lavicka ¹⁰¹, R. Lea ^{133,55}, H. Lee ¹⁰³, I. Legrand ⁴⁵, G. Legras ¹²⁵, J. Lehrbach ³⁸, A.M. Lejeune³⁵, T.M. Lelek², R.C. Lemmon ^{I,84}, I. León Monzón ¹⁰⁸, M.M. Lesch ⁹⁴, E.D. Lesser ¹⁸, P. Lévai ⁴⁶, M. Li⁶, P. Li¹⁰, X. Li¹⁰, B.E. Liang-gilman ¹⁸, J. Lien ¹²⁰, R. Lietava ⁹⁹, I. Likmeta ¹¹⁵, B. Lim ²⁴, S.H. Lim ¹⁶, V. Lindenstruth ³⁸, C. Lippmann ⁹⁶, D.H. Liu ⁶, J. Liu ¹¹⁸, G.S.S. Liveraro ¹¹⁰, I.M. Lofnes ²⁰, C. Loizides ⁸⁶, S. Lokos ¹⁰⁶, J. Lömker ⁵⁹, X. Lopez ¹²⁶, E. López Torres ⁷, C. Lotteau¹²⁷, P. Lu ^{96,119}, Z. Lu ¹⁰, F.V. Lugo ⁶⁷, J.R. Luhder ¹²⁵, G. Luparello ⁵⁷, Y.G. Ma ³⁹, M. Mager ³², A. Maire ¹²⁸, E.M. Majerz², M.V. Makariev ³⁶, M. MalaeV ¹⁴⁰, G. Malfattore ²⁵, N.M. Malik ⁹⁰, S.K. Malik ⁹⁰, D. Mallick ¹³⁰, N. Mallick ^{116,48}, G. Mandaglio ^{30,53}, S.K. Mandal ⁷⁸, A. Manea ⁶³, V. Manko ¹⁴⁰, F. Manso ¹²⁶, V. Manzari ⁵⁰, Y. Mao ⁶, R.W. Marcjan ², G.V. Margagliotti ²³, A. Margotti ⁵¹, A. Marín ⁹⁶, C. Markert ¹⁰⁷, C.F.B. Marquez³¹, P. Martinengo ³², M.I. Martínez ⁴⁴, G. Martínez García ¹⁰², M.P.P. Martins ¹⁰⁹, S. Masciocchi ⁹⁶, M. Masera ²⁴, A. Masoni ⁵², L. Massacrier ¹³⁰, O. Massen ⁵⁹, A. Mastroserio ^{131,50}, S. Mattiazzi ²⁷, A. Matyja ¹⁰⁶, F. Mazzaschi ^{32,24}, M. Mazzilli ¹¹⁵, Y. Melikyan ⁴³, M. Melo ¹⁰⁹, A. Menchaca-Rocha ⁶⁷, J.E.M. Mendez ⁶⁵, E. Meninno ¹⁰¹, A.S. Menon ¹¹⁵, M.W. Menzel^{32,93}, M. Meres ¹³, L. Micheletti ³², D. Mihai¹¹², D.L. Mihaylov ⁹⁴, K. Mikhaylov ^{141,140}, N. Minafra ¹¹⁷, D. Miśkowiec ⁹⁶, A. Modak ¹³³, B. Mohanty⁷⁹, M. Mohisin Khan ^{VI,15}, M.A. Molander ⁴³, M.M. Mondal ⁷⁹, S. Monira ¹³⁵, C. Mordasini ¹¹⁶, D.A. Moreira De Godoy ¹²⁵, I. Morozov ¹⁴⁰, A. Morsch ³², T. Mrnjavac ³², V. Muccifora ⁴⁹, S. Muhuri ¹³⁴, J.D. Mulligan ⁷³, A. Mulliri ²², M.G. Munhoz ¹⁰⁹, R.H. Munzer ⁶⁴, H. Murakami ¹²³, S. Murray ¹¹³, L. Musa ³², J. Musinsky ⁶⁰, J.W. Myrcha ¹³⁵, B. Naik ¹²², A.I. Nambrath ¹⁸, B.K. Nandi ⁴⁷, R. Nania

Velasquez ⁶⁵, J. Otwinowski ¹⁰⁶, M. Oya⁹¹, K. Oyama ⁷⁵, S. Padhan ⁴⁷, D. Pagano ^{133,55}, G. Paic̃ ⁶⁵,
 S. Paisano-Guzman ⁴⁴, A. Palasciano ⁵⁰, I. Panasenko⁷⁴, S. Panebianco ¹²⁹, C. Pantouvakis ²⁷,
 H. Park ¹²⁴, J. Park ¹²⁴, S. Park ¹⁰³, J.E. Parkkila ³², Y. Patley ⁴⁷, R.N. Patra⁵⁰, B. Paul ¹³⁴, H. Pei ⁶,
 T. Peitzmann ⁵⁹, X. Peng ¹¹, M. Pennisi ²⁴, S. Perciballi ²⁴, D. Peresunko ¹⁴⁰, G.M. Perez ⁷,
 Y. Pestov¹⁴⁰, M.T. Petersen⁸², V. Petrov ¹⁴⁰, M. Petrovici ⁴⁵, S. Piano ⁵⁷, M. Pikna ¹³, P. Pillot ¹⁰²,
 O. Pinazza ^{51,32}, L. Pinsky¹¹⁵, C. Pinto ⁹⁴, S. Pisano ⁴⁹, M. Płoskoń ⁷³, M. Planinic⁸⁸, F. Pliquett⁶⁴,
 D.K. Plociennik ², M.G. Poghosyan ⁸⁶, B. Polichtchouk ¹⁴⁰, S. Politano ²⁹, N. Poljak ⁸⁸, A. Pop ⁴⁵,
 S. Porteboeuf-Houssais ¹²⁶, V. Pozdniakov ^{1,141}, I.Y. Pozos ⁴⁴, K.K. Pradhan ⁴⁸, S.K. Prasad ⁴,
 S. Prasad ⁴⁸, R. Preghenella ⁵¹, F. Prino ⁵⁶, C.A. Pruneau ¹³⁶, I. Pshenichnov ¹⁴⁰, M. Puccio ³²,
 S. Pucillo ²⁴, S. Qiu ⁸³, L. Quaglia ²⁴, A.M.K. Radhakrishnan⁴⁸, S. Ragoni ¹⁴, A. Rai ¹³⁷,
 A. Rakotozafindrabe ¹²⁹, L. Ramello ^{132,56}, M. Rasa ²⁶, S.S. Rasanen ⁴³, R. Rath ⁵¹, M.P. Rauch ²⁰,
 I. Ravasenga ³², K.F. Read ^{86,121}, C. Reckziegel ¹¹¹, A.R. Redelbach ³⁸, K. Redlich ^{VII,78},
 C.A. Reetz ⁹⁶, H.D. Regules-Medel⁴⁴, A. Rehman²⁰, F. Reidt ³², H.A. Reme-Ness ³⁴, K. Reygers ⁹³,
 A. Riabov ¹⁴⁰, V. Riabov ¹⁴⁰, R. Ricci ²⁸, M. Richter ²⁰, A.A. Riedel ⁹⁴, W. Riegler ³²,
 A.G. Riffero ²⁴, M. Rignanese ²⁷, C. Ripoli²⁸, C. Ristea ⁶³, M.V. Rodriguez ³², M. Rodriguez
 Cahuantzi ⁴⁴, S.A. Rodriguez Ramirez ⁴⁴, K. Roed ¹⁹, R. Rogalev ¹⁴⁰, E. Rogochaya ¹⁴¹,
 T.S. Rogoschinski ⁶⁴, D. Rohr ³², D. Rohrich ²⁰, S. Rojas Torres ³⁵, P.S. Rokita ¹³⁵, G. Romanenko ²⁵,
 F. Ronchetti ³², E.D. Rosas⁶⁵, K. Roslon ¹³⁵, A. Rossi ⁵⁴, A. Roy ⁴⁸, S. Roy ⁴⁷, N. Rubini ^{51,25},
 J.A. Rudolph⁸³, D. Ruggiano ¹³⁵, R. Rui ²³, P.G. Russek ², R. Russo ⁸³, A. Rustamov ⁸⁰,
 E. Ryabinkin ¹⁴⁰, Y. Ryabov ¹⁴⁰, A. Rybicki ¹⁰⁶, J. Ryu ¹⁶, W. Rzesza ¹³⁵, B. Sabiu⁵¹, S. Sadovsky ¹⁴⁰,
 J. Saetre ²⁰, S. Saha ⁷⁹, B. Sahoo ⁴⁸, R. Sahoo ⁴⁸, S. Sahoo⁶¹, D. Sahu ⁴⁸, P.K. Sahu ⁶¹, J. Saini ¹³⁴,
 K. Sajdakova³⁷, S. Sakai ¹²⁴, M.P. Salvan ⁹⁶, S. Sambyal ⁹⁰, D. Samitz ¹⁰¹, I. Sanna ^{32,94},
 T.B. Saramela¹⁰⁹, D. Sarkar ⁸², P. Sarma ⁴¹, V. Sarritzu ²², V.M. Sarti ⁹⁴, M.H.P. Sas ³², S. Sawan ⁷⁹,
 E. Scapparone ⁵¹, J. Schambach ⁸⁶, H.S. Scheid ⁶⁴, C. Schiaua ⁴⁵, R. Schicker ⁹³, F. Schleppe ⁹³,
 A. Schmah⁹⁶, C. Schmidt ⁹⁶, M.O. Schmidt ³², M. Schmidt⁹², N.V. Schmidt ⁸⁶, A.R. Schmier ¹²¹,
 R. Schotter ^{101,128}, A. Schroter ³⁸, J. Schukraft ³², K. Schweda ⁹⁶, G. Scioli ²⁵, E. Scomparin ⁵⁶,
 J.E. Seger ¹⁴, Y. Sekiguchi¹²³, D. Sekihata ¹²³, M. Selina ⁸³, I. Selyuzhenkov ⁹⁶, S. Senyukov ¹²⁸,
 J.J. Seo ⁹³, D. Serebryakov ¹⁴⁰, L. Serkin ⁶⁵, L. ˇSerksnyte ⁹⁴, A. Sevcenco ⁶³, T.J. Shaba ⁶⁸,
 A. Shabetai ¹⁰², R. Shahoyan³², A. Shangaraev ¹⁴⁰, B. Sharma ⁹⁰, D. Sharma ⁴⁷, H. Sharma ⁵⁴,
 M. Sharma ⁹⁰, S. Sharma ⁷⁵, S. Sharma ⁹⁰, U. Sharma ⁹⁰, A. Shatat ¹³⁰, O. Sheibani^{136,115},
 K. Shigaki ⁹¹, M. Shimomura⁷⁶, J. Shin¹², S. Shirinkin ¹⁴⁰, Q. Shou ³⁹, Y. Sibiriak ¹⁴⁰, S. Siddhanta ⁵²,
 T. Siemiarczuk ⁷⁸, T.F. Silva ¹⁰⁹, D. Silvermyr ⁷⁴, T. Simantathammakul¹⁰⁴, R. Simeonov ³⁶, B. Singh⁹⁰,
 B. Singh ⁹⁴, K. Singh ⁴⁸, R. Singh ⁷⁹, R. Singh ⁹⁰, R. Singh ^{54,96}, S. Singh ¹⁵, V.K. Singh ¹³⁴,
 V. Singhal ¹³⁴, T. Sinha ⁹⁸, B. Sitar ¹³, M. Sitta ^{132,56}, T.B. Skaali¹⁹, G. Skorodumovs ⁹³,
 N. Smirnov ¹³⁷, R.J.M. Snellings ⁵⁹, E.H. Solheim ¹⁹, C. Sonnabend ^{32,96}, J.M. Sonneveld ⁸³,
 F. Soramel ²⁷, A.B. Soto-hernandez ⁸⁷, R. Spijkers ⁸³, I. Sputowska ¹⁰⁶, J. Staa ⁷⁴, J. Stachel ⁹³,
 I. Stan ⁶³, P.J. Steffanic ¹²¹, T. Stellhorn¹²⁵, S.F. Stiefelmaier ⁹³, D. Stocco ¹⁰², I. Storehaug ¹⁹,
 N.J. Strangmann ⁶⁴, P. Stratmann ¹²⁵, S. Strazzi ²⁵, A. Sturniolo ^{30,53}, C.P. Stylianidis⁸³,
 A.A.P. Suaide ¹⁰⁹, C. Suire ¹³⁰, A. Suiu^{32,112}, M. Sukhanov ¹⁴⁰, M. Suljic ³², R. Sultanov ¹⁴⁰,
 V. Sumberia ⁹⁰, S. Sumowidagdo ⁸¹, M. Szymkowski ¹³⁵, L.H. Tabares⁷, S.F. Taghavi ⁹⁴,
 J. Takahashi ¹¹⁰, G.J. Tambave ⁷⁹, S. Tang ⁶, Z. Tang ¹¹⁹, J.D. Tapia Takaki ¹¹⁷, N. Tapus¹¹²,
 L.A. Tarasovicova ³⁷, M.G. Tarzila ⁴⁵, A. Tauro ³², A. Tavira Garcia ¹³⁰, G. Tejada Munoz ⁴⁴,
 L. Terlizzi ²⁴, C. Terrevoli ⁵⁰, S. Thakur ⁴, M. Thogersen¹⁹, D. Thomas ¹⁰⁷, A. Tikhonov ¹⁴⁰,
 N. Tiltmann ^{32,125}, A.R. Timmins ¹¹⁵, M. Tkacik¹⁰⁵, T. Tkacik ¹⁰⁵, A. Toia ⁶⁴, R. Tokumoto⁹¹,
 S. Tomassini²⁵, K. Tomohiro⁹¹, N. Topilskaya ¹⁴⁰, M. Toppi ⁴⁹, V.V. Torres ¹⁰², A.G. Torres Ramos ³¹,
 A. Trifiro ^{30,53}, T. Triloki⁹⁵, A.S. Triolo ^{32,30,53}, S. Tripathy ³², T. Tripathy ⁴⁷, S. Trogolo ²⁴,
 V. Trubnikov ³, W.H. Trzaska ¹¹⁶, T.P. Trzcinski ¹³⁵, C. Tsolanta¹⁹, R. Tu³⁹, A. Tumkin ¹⁴⁰, R. Turrisi ⁵⁴,
 T.S. Tveter ¹⁹, K. Ullaland ²⁰, B. Ulukutlu ⁹⁴, S. Upadhyaya ¹⁰⁶, A. Uras ¹²⁷, G.L. Usai ²², M. Vala³⁷,
 N. Valle ⁵⁵, L.V.R. van Doremalen⁵⁹, M. van Leeuwen ⁸³, C.A. van Veen ⁹³, R.J.G. van Weelden ⁸³,
 P. Vande Vyvre ³², D. Varga ⁴⁶, Z. Varga ^{137,46}, P. Vargas Torres⁶⁵, M. Vasileiou ⁷⁷, A. Vasiliev ^{I,140},
 O. Vazquez Doce ⁴⁹, O. Vazquez Rueda ¹¹⁵, V. Vechernin ¹⁴⁰, E. Vercellin ²⁴, R. Verma ⁴⁷,
 R. Vertesi ⁴⁶, M. Verweij ⁵⁹, L. Vickovic³³, Z. Vilakazi¹²², O. Villalobos Baillie ⁹⁹, A. Villani ²³,
 A. Vinogradov ¹⁴⁰, T. Virgili ²⁸, M.M.O. Virta ¹¹⁶, A. Vodopyanov ¹⁴¹, B. Volkel ³², M.A. Volkl ⁹³,
 S.A. Voloshin ¹³⁶, G. Volpe ³¹, B. von Haller ³², I. Vorobyev ³², N. Vozniuk ¹⁴⁰, J. Vrlakova ³⁷,
 J. Wan³⁹, C. Wang ³⁹, D. Wang ^{39</}

G. Wilk⁷⁸, J. Wilkinson⁹⁶, G.A. Willems¹²⁵, B. Windelband⁹³, M. Winn¹²⁹, J.R. Wright¹⁰⁷, W. Wu³⁹, Y. Wu¹¹⁹, Z. Xiong¹¹⁹, R. Xu⁶, A. Yadav⁴², A.K. Yadav¹³⁴, Y. Yamaguchi⁹¹, S. Yang²⁰, S. Yano⁹¹, E.R. Yeats¹⁸, Z. Yin⁶, I.-K. Yoo¹⁶, J.H. Yoon⁵⁸, H. Yu¹², S. Yuan²⁰, A. Yuncu⁹³, V. Zaccaro²³, C. Zampolli³², F. Zanone⁹³, N. Zardoshti³², A. Zarochentsev¹⁴⁰, P. Závada⁶², N. Zaviyalov¹⁴⁰, M. Zhalov¹⁴⁰, B. Zhang^{93,6}, C. Zhang¹²⁹, L. Zhang³⁹, M. Zhang^{126,6}, M. Zhang⁶, S. Zhang³⁹, X. Zhang⁶, Y. Zhang¹¹⁹, Z. Zhang⁶, M. Zhao¹⁰, V. Zhrebchevskii¹⁴⁰, Y. Zhi¹⁰, D. Zhou⁶, Y. Zhou⁸², J. Zhu^{54,6}, S. Zhu¹¹⁹, Y. Zhu⁶, S.C. Zugravel⁵⁶, N. Zurlo^{133,55}

Affiliation Notes

^I Deceased

^{II} Also at: Max-Planck-Institut für Physik, Munich, Germany

^{III} Also at: Italian National Agency for New Technologies, Energy and Sustainable Economic Development (ENEA), Bologna, Italy

^{IV} Also at: Dipartimento DET del Politecnico di Torino, Turin, Italy

^V Also at: Yildiz Technical University, Istanbul, Türkiye

^{VI} Also at: Department of Applied Physics, Aligarh Muslim University, Aligarh, India

^{VII} Also at: Institute of Theoretical Physics, University of Wrocław, Poland

^{VIII} Also at: An institution covered by a cooperation agreement with CERN

Collaboration Institutes

¹ A.I. Alikhanyan National Science Laboratory (Yerevan Physics Institute) Foundation, Yerevan, Armenia

² AGH University of Krakow, Cracow, Poland

³ Bogolyubov Institute for Theoretical Physics, National Academy of Sciences of Ukraine, Kiev, Ukraine

⁴ Bose Institute, Department of Physics and Centre for Astroparticle Physics and Space Science (CAPSS), Kolkata, India

⁵ California Polytechnic State University, San Luis Obispo, California, United States

⁶ Central China Normal University, Wuhan, China

⁷ Centro de Aplicaciones Tecnológicas y Desarrollo Nuclear (CEADEN), Havana, Cuba

⁸ Centro de Investigación y de Estudios Avanzados (CINVESTAV), Mexico City and Mérida, Mexico

⁹ Chicago State University, Chicago, Illinois, United States

¹⁰ China Institute of Atomic Energy, Beijing, China

¹¹ China University of Geosciences, Wuhan, China

¹² Chungbuk National University, Cheongju, Republic of Korea

¹³ Comenius University Bratislava, Faculty of Mathematics, Physics and Informatics, Bratislava, Slovak Republic

¹⁴ Creighton University, Omaha, Nebraska, United States

¹⁵ Department of Physics, Aligarh Muslim University, Aligarh, India

¹⁶ Department of Physics, Pusan National University, Pusan, Republic of Korea

¹⁷ Department of Physics, Sejong University, Seoul, Republic of Korea

¹⁸ Department of Physics, University of California, Berkeley, California, United States

¹⁹ Department of Physics, University of Oslo, Oslo, Norway

²⁰ Department of Physics and Technology, University of Bergen, Bergen, Norway

²¹ Dipartimento di Fisica, Università di Pavia, Pavia, Italy

²² Dipartimento di Fisica dell'Università and Sezione INFN, Cagliari, Italy

²³ Dipartimento di Fisica dell'Università and Sezione INFN, Trieste, Italy

²⁴ Dipartimento di Fisica dell'Università and Sezione INFN, Turin, Italy

²⁵ Dipartimento di Fisica e Astronomia dell'Università and Sezione INFN, Bologna, Italy

²⁶ Dipartimento di Fisica e Astronomia dell'Università and Sezione INFN, Catania, Italy

²⁷ Dipartimento di Fisica e Astronomia dell'Università and Sezione INFN, Padova, Italy

²⁸ Dipartimento di Fisica 'E.R. Caianiello' dell'Università and Gruppo Collegato INFN, Salerno, Italy

²⁹ Dipartimento DISAT del Politecnico and Sezione INFN, Turin, Italy

³⁰ Dipartimento di Scienze MIFT, Università di Messina, Messina, Italy

³¹ Dipartimento Interateneo di Fisica 'M. Merlin' and Sezione INFN, Bari, Italy

³² European Organization for Nuclear Research (CERN), Geneva, Switzerland

³³ Faculty of Electrical Engineering, Mechanical Engineering and Naval Architecture, University of Split, Split, Croatia

- ³⁴ Faculty of Engineering and Science, Western Norway University of Applied Sciences, Bergen, Norway
- ³⁵ Faculty of Nuclear Sciences and Physical Engineering, Czech Technical University in Prague, Prague, Czech Republic
- ³⁶ Faculty of Physics, Sofia University, Sofia, Bulgaria
- ³⁷ Faculty of Science, P.J. Šafárik University, Košice, Slovak Republic
- ³⁸ Frankfurt Institute for Advanced Studies, Johann Wolfgang Goethe-Universität Frankfurt, Frankfurt, Germany
- ³⁹ Fudan University, Shanghai, China
- ⁴⁰ Gangneung-Wonju National University, Gangneung, Republic of Korea
- ⁴¹ Gauhati University, Department of Physics, Guwahati, India
- ⁴² Helmholtz-Institut für Strahlen- und Kernphysik, Rheinische Friedrich-Wilhelms-Universität Bonn, Bonn, Germany
- ⁴³ Helsinki Institute of Physics (HIP), Helsinki, Finland
- ⁴⁴ High Energy Physics Group, Universidad Autónoma de Puebla, Puebla, Mexico
- ⁴⁵ Horia Hulubei National Institute of Physics and Nuclear Engineering, Bucharest, Romania
- ⁴⁶ HUN-REN Wigner Research Centre for Physics, Budapest, Hungary
- ⁴⁷ Indian Institute of Technology Bombay (IIT), Mumbai, India
- ⁴⁸ Indian Institute of Technology Indore, Indore, India
- ⁴⁹ INFN, Laboratori Nazionali di Frascati, Frascati, Italy
- ⁵⁰ INFN, Sezione di Bari, Bari, Italy
- ⁵¹ INFN, Sezione di Bologna, Bologna, Italy
- ⁵² INFN, Sezione di Cagliari, Cagliari, Italy
- ⁵³ INFN, Sezione di Catania, Catania, Italy
- ⁵⁴ INFN, Sezione di Padova, Padova, Italy
- ⁵⁵ INFN, Sezione di Pavia, Pavia, Italy
- ⁵⁶ INFN, Sezione di Torino, Turin, Italy
- ⁵⁷ INFN, Sezione di Trieste, Trieste, Italy
- ⁵⁸ Inha University, Incheon, Republic of Korea
- ⁵⁹ Institute for Gravitational and Subatomic Physics (GRASP), Utrecht University/Nikhef, Utrecht, Netherlands
- ⁶⁰ Institute of Experimental Physics, Slovak Academy of Sciences, Košice, Slovak Republic
- ⁶¹ Institute of Physics, Homi Bhabha National Institute, Bhubaneswar, India
- ⁶² Institute of Physics of the Czech Academy of Sciences, Prague, Czech Republic
- ⁶³ Institute of Space Science (ISS), Bucharest, Romania
- ⁶⁴ Institut für Kernphysik, Johann Wolfgang Goethe-Universität Frankfurt, Frankfurt, Germany
- ⁶⁵ Instituto de Ciencias Nucleares, Universidad Nacional Autónoma de México, Mexico City, Mexico
- ⁶⁶ Instituto de Física, Universidade Federal do Rio Grande do Sul (UFRGS), Porto Alegre, Brazil
- ⁶⁷ Instituto de Física, Universidad Nacional Autónoma de México, Mexico City, Mexico
- ⁶⁸ iThemba LABS, National Research Foundation, Somerset West, South Africa
- ⁶⁹ Jeonbuk National University, Jeonju, Republic of Korea
- ⁷⁰ Johann-Wolfgang-Goethe Universität Frankfurt Institut für Informatik, Fachbereich Informatik und Mathematik, Frankfurt, Germany
- ⁷¹ Korea Institute of Science and Technology Information, Daejeon, Republic of Korea
- ⁷² Laboratoire de Physique Subatomique et de Cosmologie, Université Grenoble-Alpes, CNRS-IN2P3, Grenoble, France
- ⁷³ Lawrence Berkeley National Laboratory, Berkeley, California, United States
- ⁷⁴ Lund University Department of Physics, Division of Particle Physics, Lund, Sweden
- ⁷⁵ Nagasaki Institute of Applied Science, Nagasaki, Japan
- ⁷⁶ Nara Women's University (NWU), Nara, Japan
- ⁷⁷ National and Kapodistrian University of Athens, School of Science, Department of Physics, Athens, Greece
- ⁷⁸ National Centre for Nuclear Research, Warsaw, Poland
- ⁷⁹ National Institute of Science Education and Research, Homi Bhabha National Institute, Jatni, India
- ⁸⁰ National Nuclear Research Center, Baku, Azerbaijan
- ⁸¹ National Research and Innovation Agency - BRIN, Jakarta, Indonesia
- ⁸² Niels Bohr Institute, University of Copenhagen, Copenhagen, Denmark
- ⁸³ Nikhef, National institute for subatomic physics, Amsterdam, Netherlands
- ⁸⁴ Nuclear Physics Group, STFC Daresbury Laboratory, Daresbury, United Kingdom
- ⁸⁵ Nuclear Physics Institute of the Czech Academy of Sciences, Husinec-Řež, Czech Republic

- ⁸⁶ Oak Ridge National Laboratory, Oak Ridge, Tennessee, United States
⁸⁷ Ohio State University, Columbus, Ohio, United States
⁸⁸ Physics department, Faculty of science, University of Zagreb, Zagreb, Croatia
⁸⁹ Physics Department, Panjab University, Chandigarh, India
⁹⁰ Physics Department, University of Jammu, Jammu, India
⁹¹ Physics Program and International Institute for Sustainability with Knotted Chiral Meta Matter (SKCM2), Hiroshima University, Hiroshima, Japan
⁹² Physikalisches Institut, Eberhard-Karls-Universität Tübingen, Tübingen, Germany
⁹³ Physikalisches Institut, Ruprecht-Karls-Universität Heidelberg, Heidelberg, Germany
⁹⁴ Physik Department, Technische Universität München, Munich, Germany
⁹⁵ Politecnico di Bari and Sezione INFN, Bari, Italy
⁹⁶ Research Division and ExtreMe Matter Institute EMMI, GSI Helmholtzzentrum für Schwerionenforschung GmbH, Darmstadt, Germany
⁹⁷ Saga University, Saga, Japan
⁹⁸ Saha Institute of Nuclear Physics, Homi Bhabha National Institute, Kolkata, India
⁹⁹ School of Physics and Astronomy, University of Birmingham, Birmingham, United Kingdom
¹⁰⁰ Sección Física, Departamento de Ciencias, Pontificia Universidad Católica del Perú, Lima, Peru
¹⁰¹ Stefan Meyer Institut für Subatomare Physik (SMI), Vienna, Austria
¹⁰² SUBATECH, IMT Atlantique, Nantes Université, CNRS-IN2P3, Nantes, France
¹⁰³ Sungkyunkwan University, Suwon City, Republic of Korea
¹⁰⁴ Suranaree University of Technology, Nakhon Ratchasima, Thailand
¹⁰⁵ Technical University of Košice, Košice, Slovak Republic
¹⁰⁶ The Henryk Niewodniczanski Institute of Nuclear Physics, Polish Academy of Sciences, Cracow, Poland
¹⁰⁷ The University of Texas at Austin, Austin, Texas, United States
¹⁰⁸ Universidad Autónoma de Sinaloa, Culiacán, Mexico
¹⁰⁹ Universidade de São Paulo (USP), São Paulo, Brazil
¹¹⁰ Universidade Estadual de Campinas (UNICAMP), Campinas, Brazil
¹¹¹ Universidade Federal do ABC, Santo Andre, Brazil
¹¹² Universitatea Nationala de Stiinta si Tehnologie Politehnica Bucuresti, Bucharest, Romania
¹¹³ University of Cape Town, Cape Town, South Africa
¹¹⁴ University of Derby, Derby, United Kingdom
¹¹⁵ University of Houston, Houston, Texas, United States
¹¹⁶ University of Jyväskylä, Jyväskylä, Finland
¹¹⁷ University of Kansas, Lawrence, Kansas, United States
¹¹⁸ University of Liverpool, Liverpool, United Kingdom
¹¹⁹ University of Science and Technology of China, Hefei, China
¹²⁰ University of South-Eastern Norway, Kongsberg, Norway
¹²¹ University of Tennessee, Knoxville, Tennessee, United States
¹²² University of the Witwatersrand, Johannesburg, South Africa
¹²³ University of Tokyo, Tokyo, Japan
¹²⁴ University of Tsukuba, Tsukuba, Japan
¹²⁵ Universität Münster, Institut für Kernphysik, Münster, Germany
¹²⁶ Université Clermont Auvergne, CNRS/IN2P3, LPC, Clermont-Ferrand, France
¹²⁷ Université de Lyon, CNRS/IN2P3, Institut de Physique des 2 Infinis de Lyon, Lyon, France
¹²⁸ Université de Strasbourg, CNRS, IPHC UMR 7178, F-67000 Strasbourg, France, Strasbourg, France
¹²⁹ Université Paris-Saclay, Centre d'Etudes de Saclay (CEA), IRFU, Département de Physique Nucléaire (DPhN), Saclay, France
¹³⁰ Université Paris-Saclay, CNRS/IN2P3, IJCLab, Orsay, France
¹³¹ Università degli Studi di Foggia, Foggia, Italy
¹³² Università del Piemonte Orientale, Vercelli, Italy
¹³³ Università di Brescia, Brescia, Italy
¹³⁴ Variable Energy Cyclotron Centre, Homi Bhabha National Institute, Kolkata, India
¹³⁵ Warsaw University of Technology, Warsaw, Poland
¹³⁶ Wayne State University, Detroit, Michigan, United States
¹³⁷ Yale University, New Haven, Connecticut, United States
¹³⁸ Yildiz Technical University, Istanbul, Turkey

¹³⁹ Yonsei University, Seoul, Republic of Korea

¹⁴⁰ Affiliated with an institute covered by a cooperation agreement with CERN

¹⁴¹ Affiliated with an international laboratory covered by a cooperation agreement with CERN.